



# Origins of the Inverse Electrocaloric Effect

Anna Grünebohm,<sup>\*,[a]</sup> Yang-Bin Ma,<sup>\*,[b]</sup> Madhura Marathe,<sup>[c]</sup> Bai-Xiang Xu,<sup>[b]</sup> Karsten Albe,<sup>[b]</sup> Constanze Kalcher,<sup>[b]</sup> Kai-Christian Meyer,<sup>[b]</sup> Vladimir V. Shvartsman,<sup>[d]</sup> Doru C. Lupascu,<sup>[d]</sup> and Claude Ederer<sup>[e]</sup>

The occurrence of the inverse (or negative) electrocaloric effect, where the isothermal application of an electric field leads to an increase in entropy and the removal of the field decreases the entropy of the system under consideration, is discussed and analyzed. Inverse electrocaloric effects have been reported to occur in several cases, for example, at transitions between ferroelectric phases with different polarization directions, in materials with certain polar defect configurations, and in antiferroelectrics. This counterintuitive relationship between entropy and applied field is intriguing and thus of general scientific interest. The combined application of normal and inverse effects has also been suggested as a

means to achieve larger temperature differences between hot and cold reservoirs in future cooling devices. A good general understanding and the possibility to engineer inverse caloric effects in terms of temperature spans, required fields, and operating temperatures are thus of fundamental as well as technological importance. Here, the known cases of inverse electrocaloric effects are reviewed, their physical origins are discussed, and the different cases are compared to identify common aspects as well as potential differences. In all cases the inverse electrocaloric effect is related to the presence of competing phases or states that are close in energy and can easily be transformed with the applied field.

## 1. Introduction

The electrocaloric effect (ECE) describes a temperature or entropy change of a material under application of an external electric field. While the ECE has long been viewed as a rather small effect without much technological relevance, the field of electrocaloric (EC) materials has recently seen a tremendous increase in research activity, following the demonstration of a “giant” EC response in Pb(Zr,Ti)O<sub>3</sub> thin films in 2006.<sup>[1]</sup> The (indirectly) obtained adiabatic temperature change of  $\Delta T \approx 12$  K in that work has opened up the possibility to use the ECE for future applications in refrigeration and other solid state cooling devices.<sup>[2,3]</sup> Much work has been done since then, focusing on fundamental aspects, materials optimization, and possible device concepts (see, for example, Ref. [4–10] for recent reviews).

In the normal case (conventional or positive ECE), the applied field orders the electric dipoles in a dielectric material and thus lowers its entropy or, under adiabatic conditions, increases its temperature. However, under certain conditions also an inverse (or negative) ECE can occur, where the isothermal entropy change,  $\Delta S$ , is positive and the adiabatic temperature change,  $\Delta T$ , is negative under an increasing electric field.

Examples where such an inverse EC response has been observed experimentally include antiferroelectric (AFE) materials<sup>[11–13]</sup> and ferroelectric (FE) materials exhibiting transitions between different FE phases corresponding to different polarization directions.<sup>[14,15]</sup> Furthermore, an inverse caloric response has been suggested to occur for certain polar defect configurations in FE materials.<sup>[16]</sup> However, in all these

cases, the inverse effect is restricted to specific temperature and field regions.


[a] Dr. A. Grünebohm  
Faculty of Physics and Center for Nanointegration Duisburg-Essen (CENIDE)  
University of Duisburg-Essen  
47048 Duisburg (Germany)  
E-mail: anna@thp.uni-due.de


[b] Dr. Y. B. Ma, Prof. B.-X. Xu, Prof. K. Albe, C. Kalcher, Dr. K.-C. Meyer  
Institute of Materials Science  
Technische Universität Darmstadt  
64287 Darmstadt (Germany)  
E-mail: y.ma@mfm.tu-darmstadt.de


[c] Dr. M. Marathe  
Institut de Ciència de Materials de Barcelona (ICMAB-CSIC)  
Campus UAB, 08193 Bellaterra (Spain)

[d] Dr. V. V. Shvartsman, Prof. D. C. Lupascu  
Institute for Materials Science and Center for Nanointegration Duisburg-Essen (CENIDE)  
University of Duisburg-Essen  
45141 Essen (Germany)

[e] Prof. C. Ederer  
Materials Theory  
ETH Zürich  
Wolfgang-Pauli-Str. 27, 8093 Zürich (Switzerland)

 The ORCID identification number(s) for the author(s) of this article can be found under:  
<https://doi.org/10.1002/ente.201800166>.

 © 2018 The Authors. Published by Wiley-VCH Verlag GmbH & Co. KGaA. This is an open access article under the terms of the Creative Commons Attribution Non-Commercial License, which permits use, distribution and reproduction in any medium, provided the original work is properly cited, and is not used for commercial purposes.

 This publication is part of a Special Issue on “Ferroic Cooling”. To view the complete issue, visit: <http://dx.doi.org/10.1002/ente.v6.8>.

At first glance, an increase of entropy in a dipolar system under application of an external field seems rather counter intuitive. However, it has been reported that, if the external field is applied along a direction that is either non-collinear<sup>[17–22]</sup> or antiparallel<sup>[18,23–29]</sup> to the direction of the spontaneous electric polarization in a FE, the applied field can create disorder in the alignment of the electric dipoles and thus lead to an inverse ECE. Similarly, an electric field favors the FE phase with homogeneous polarization and can eventually reduce the ordering in AFE phases resulting in an inverse EC response.<sup>[30]</sup> Several suggestions have been made to utilize a combination of the conventional and inverse

ECE to achieve a larger overall temperature change ( $\Delta T$ ) and thus enable optimized EC cooling cycles.<sup>[17,23–29]</sup> On the other hand, an unintentional combination of inverse and conventional effects can also reduce the overall EC response of a system, for example, in polycrystals or in inhomogeneous materials. It is, therefore, very important to have a good understanding of the specific parameter ranges giving rise to large inverse EC responses, that is, factors such as doping level, strain, temperature, magnitude, and direction of the electric field, as well as process conditions, to avoid an unintentional compensation between normal and inverse effects and obtain the maximally possible response for future cooling applications. Furthermore, as recently discussed by Birks et al.,<sup>[31]</sup> an apparent inverse ECE can sometimes be an artifact of the measurement and data analysis methods. It is thus important to avoid such pitfalls in order to obtain reliable information about the specific conditions for which a certain material exhibits a conventional or an inverse EC response.

The purpose of this article is to review different previous reports on the inverse ECE and to identify the common features and potential differences to consolidate these findings into a comprehensive picture. We hope that this will enable more targeted future studies and optimization of the EC response with regards to potential applications.

The article is organized as follows. In Section 2, we summarize the main thermodynamic aspects and introduce the basic equations relevant for the discussion in the subsequent sections. In Section 3, we review the various systems for which the inverse effect has been observed in detail, and we discuss possible mechanisms responsible for this effect. We distinguish between ferroelectrics, where the field is reversed or non-collinear to the polarization direction; acceptor-doped ferroelectrics, where defect dipoles affect the ECE; and antiferroelectrics. In Section 4, we discuss some more general aspects of the inverse EC response such as advantages, possible disadvantages, and potential pitfalls associated with the artificial prediction of inverse response from so-called indirect measurements. Furthermore, we compare the inverse ECE with the closely related inverse magnetocaloric and elastocaloric effects. Finally, a summary and an outlook are given in Section 5.

Dr. Anna Grünebohm received her diploma in 2008 and received her Ph.D. in 2013 from the University of Duisburg-Essen (Germany) under the supervision of Prof. P. Entel. She is currently working as principle investigator in the German focus project “Ferroic cooling”. Her research interests are *ab initio* based scale-bridging simulations of functional ferroelectric, magnetic and composite materials.



Dr. Yang-Bin Ma received his B.Sc. degree in Materials Science and Technology from University of Science and Technology Beijing (China). In 2011, he obtained his M.Sc. degree in Biomaterials and Composites from AGH University of Science and Technology (Poland). From 2011 to 2012 he worked as an associate research manager for Jiangsu Xujing New Energy LTD. At present he is a scientific staff member at TU Darmstadt (Germany), where he conducted his Ph.D. studies from 2013 to 2017 working on modelling of electrocaloric materials. His current research interests are theory and multi-scale modelling of dielectrics and ferroelectrics.



Dr. Madhura Marathe received her M.Sc. from the University of Pune (India) in 2006 and Ph.D. from JNCASR, Bangalore (India) in 2013 under the supervision of Prof. S. Narasimhan. She did her initial postdoctoral research in the group of Prof. N. Spaldin with Prof. C. Ederer (ETH-Zürich). She is currently working as a Marie Skłodowska-Curie (COFUND) post-doctoral fellow at ICMA-B-CSIC, Barcelona with Prof. M. Stengel. Her research interests include application of density functional theory to study the structural properties of metallic surface alloys and ferroelectric materials as well as molecular dynamics simulations to study the finite temperature properties of ferroelectrics.



## 2. Thermodynamics

The free energy density ( $F(T, \mathbf{E})$ ), of a dielectric material can be written in terms of temperature ( $T$ ) and electric field ( $\mathbf{E}$ ). Here,  $F(T, \mathbf{E})$  can refer both to the Helmholtz free energy density ( $F = U - TS - \mathbf{E} \cdot \mathbf{P}$ ), with the specific internal energy ( $U$ ), specific entropy ( $S$ ), and electric polarization ( $\mathbf{P}$ ) as well as to the Gibbs free energy density ( $F = U - TS - \mathbf{E} \cdot \mathbf{P} - \text{tr}(\boldsymbol{\sigma}^T \cdot \boldsymbol{\eta})$ ), with stress  $\boldsymbol{\sigma}$  and strain  $\boldsymbol{\eta}$  depending on the mechanical boundary conditions.<sup>[32,33]</sup> Note that polarization and electric field are vectors, and stress and strain are tensors of rank two. Furthermore, in the following we will refer to the specific entropy, that is, the entropy per unit volume, simply as “entropy”.

Entropy and electric polarization are then defined as  $S(T, \mathbf{E}) = -\partial F / \partial T$  and  $\mathbf{P}(T, \mathbf{E}) = -\partial F / \partial \mathbf{E}$ , respectively, and a general entropy change is given by Equation (1):

$$dS = \left. \frac{\partial S}{\partial T} \right|_{\mathbf{E}} dT + \left. \frac{\partial S}{\partial \mathbf{E}} \right|_T \cdot d\mathbf{E} \quad (1)$$

Thus, under isothermal variation of the electric field ( $dT=0$ ) one obtains:

$$dS = \left. \frac{\partial S}{\partial \mathbf{E}} \right|_T \cdot d\mathbf{E} = \left. \frac{\partial \mathbf{P}}{\partial T} \right|_{\mathbf{E}} \cdot d\mathbf{E} \quad (2)$$

where the following thermodynamic Maxwell relation has been used:

$$\left. \frac{\partial S}{\partial \mathbf{E}} \right|_T = - \left. \frac{\partial^2 F}{\partial \mathbf{E} \partial T} \right|_T = \left. \frac{\partial \mathbf{P}}{\partial T} \right|_{\mathbf{E}} \quad (3)$$

Under adiabatic conditions ( $dS=0$ ), the temperature change under variation of an electric field can be obtained from Equation (1) as:

$$dT = - \left( \left. \frac{\partial S}{\partial \mathbf{E}} \right|_T \right) \left( \left. \frac{\partial S}{\partial T} \right|_{\mathbf{E}} \right)^{-1} \cdot d\mathbf{E} = - \frac{T}{C_E} \left. \frac{\partial \mathbf{P}}{\partial T} \right|_{\mathbf{E}} \cdot d\mathbf{E} \quad (4)$$

where  $C_E = T \partial S / \partial T|_{\mathbf{E}}$  is the specific heat at constant electric field and again the Maxwell relation [Eq. (3)] has been used. Note that entropy and temperature changes depend on the scalar product of  $\partial \mathbf{P} / \partial T$  and  $d\mathbf{E}$ , [cf. Eqs. (2) and (4)]. In the following, we only consider processes where the electric field is varied along a fixed direction, and then  $P$  and  $E$  refer to the components of  $\mathbf{P}$  and  $\mathbf{E}$  along the (positive) field direction. A negative  $E$  thus indicates a reversal of the field along the given axis.

By integrating Equations (2) and (4) from an initial field  $E_{\text{init}}$  to a final field  $E_{\text{end}}$ , one obtains the total isothermal EC entropy change ( $\Delta S$ ) and the total adiabatic EC temperature change ( $\Delta T$ ) from the temperature and field dependence of the electric polarization  $P(T, E)$  as

$$\Delta S = \int_{E_{\text{init}}}^{E_{\text{end}}} \left. \frac{\partial P}{\partial T} \right|_E dE \quad (5)$$

and

$$\Delta T = - \int_{E_{\text{init}}}^{E_{\text{end}}} \frac{T}{C_E(T)} \left. \frac{\partial P}{\partial T} \right|_E dE \quad (6)$$

It can easily be seen from Equations (5) and (6) that for increasing field, that is, positive  $dE$ , the conventional ECE is related to a negative slope of  $P(T)$ : for decreasing polarization with increasing temperature ( $(\partial P / \partial T)_E < 0$ ), while a positive slope of  $P(T)$  would correspond to an inverse ECE. On the other hand, as usually  $P$  and  $\partial P / \partial T$  have opposite signs,

an inverse ECE is also possible if  $\mathbf{P}$  and  $\mathbf{E}$  are antiparallel, for example, for a reversed field in a poled ferroelectric (such that  $(\partial P / \partial T)_E$  and  $dE$  have the same sign).

Sometimes it is instructive to separate the total entropy change into a part related to the dipolar degrees of freedom that give rise to the ferroelectric polarization ( $\Delta S_{\text{dip}}$ ) and the remaining vibrational degrees of freedom ( $\Delta S_{\text{latt}}$ ).<sup>[9,30]</sup> Under adiabatic (and reversible) conditions, the change in entropy of the dipolar system (caused by application or removal of an external field) is then redistributed to the remaining degrees of freedom [Eqs. (7)-(9)]:

$$\Delta S_{\text{dip}} = -\Delta S_{\text{latt}} \quad (7)$$

$$= - \int_{T_{\text{init}}}^{T_{\text{end}}} \frac{C_{\text{latt}}}{T} dT \quad (8)$$

$$\approx -C_{\text{latt}} \ln(T_{\text{end}} / T_{\text{init}}) \quad (9)$$

Here,  $C_{\text{latt}}$  is the specific heat capacity related to the non-dipolar degrees of freedom, which, by its definition, is only weakly temperature and field dependent in the range of interest. Thus, a decrease of the dipolar entropy ( $\Delta S_{\text{dip}} < 0$ ) corresponds to  $T_{\text{end}} > T_{\text{init}}$ , that is, heating of the system, whereas an increase in dipolar entropy ( $\Delta S_{\text{dip}} > 0$ ) results in cooling ( $T_{\text{end}} < T_{\text{init}}$ ), consistent with Equations (5) and (6).

For an intuitive interpretation of the ECE in a simple ferroelectric (or paraelectric) phase under a collinear field, one can also use Landau theory and expand the (dipolar) free energy density with respect to  $P$ :<sup>[9,28,30]</sup>

$$F_{\text{dip}} = F_0 + \frac{1}{2} a_0 (T - T_C) P^2 + \frac{1}{4} b P^4 - EP \quad (10)$$

where  $a_0$  and  $b$  are material-dependent parameters, and  $T_C$  is the Curie temperature. The field-induced change of the dipolar entropy is then given by:

$$\Delta S_{\text{dip}} = -\frac{1}{2} a_0 (P_{\text{end}}^2 - P_{\text{init}}^2) \quad (11)$$

that is, the change in the dipolar entropy is essentially determined by the change in the absolute value of  $P$ . Note, that Equation (10) does not apply to more complex cases such as transitions between FE phases with different polarization directions.

As discussed in more detail in Section 3, the largest ECE is typically observed at ferroelectric phase transitions, which are often of first order where  $P(T)$  exhibits an abrupt jump and  $\partial P / \partial T$  is thus ill defined. Nevertheless, one can generalize Equation (5) for such cases by splitting the polarization into a part that varies smoothly with  $T$  and  $E$  ( $\tilde{P}(T, E)$ ) and a discontinuous jump ( $\Delta P(E, (T))$ ), which occurs at the temperature-dependent transition field  $E_i(T)$  or, equivalently, at the field-dependent transition temperature  $T_i(E)$ .<sup>[20,34,35]</sup>

$$P(T, E) = \tilde{P}(T, E) + \Delta P(E_i(T))\Theta(T - T_i(E)) \quad (12)$$

Here,  $\Theta(T - T_i(E))$  represents the Heaviside step function, which is 0 for  $T - T_i(E) < 0$  and 1 for  $T - T_i(E) > 0$ . Assuming that  $E_i(T)$  (or  $T_i(E)$ , respectively) is uniquely defined in the considered temperature and field range, one can substitute Equation (12) into Equation (5), thereby taking the derivative with respect to  $T$ , and one can show that the total entropy change is given as the sum of two contributions as follows:

$$\Delta S = \Delta \tilde{S} + \Delta S_{\text{LH}} \quad (13)$$

where  $\Delta \tilde{S}$  is obtained from the continuous part  $\tilde{P}(T, E)$  via Equation (5) and  $\Delta S_{\text{LH}}$  is the contribution stemming from the discontinuous jump  $\Delta P$  at the first order phase transition.  $\Delta S_{\text{LH}}$  is related to the latent heat of the first order phase transition which is given by the following Clausius–Clapeyron equation:

$$\Delta S_{\text{LH}} = \Delta P(E_i(T)) \left| \frac{dE_i}{dT} \right| \quad (14)$$

It should be noted that within the coexistence range of a first order phase transition the state of the system (and thus the measured ECE) is not fully determined by the values of  $E$  and  $T$  but depends on the history of the sample, that is, on the preceding heat and field treatment. Thus, a well-defined initial state is crucial for obtaining meaningful EC entropy and temperature changes. Furthermore, in such cases, the EC response can be irreversible if the system (or parts of it) is trapped inside the coexistence range, see Section 3.1.2. The same is true within the FE phase where the system can exhibit a field hysteresis (see, e.g., Figure 1).

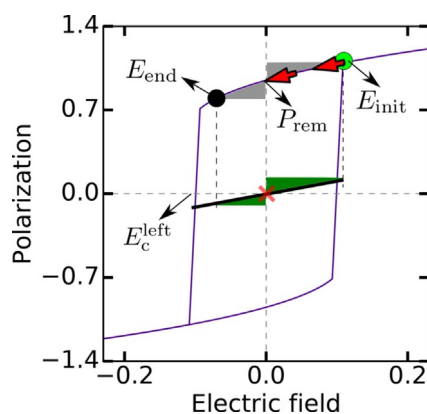


**Figure 1.** Schematic picture of a ferroelectric hysteresis loop for collinear field and polarization. If the field is ramped from  $E_{\text{init}} > 0$  (lime dot) to a negative  $E_{\text{end}}$  (black dot), it does the total work (per unit volume)  $W_{\text{total}} = \int_{P_{\text{init}}}^{P_{\text{end}}} E dP$  (gray area). The work can be separated into work losses  $W_{\text{loss}}$  and the reversible work (green area) defined as the work done on the reversible polarization  $P_r$  (black line crossing the center of the hysteresis),  $W_r = \int_{P_{\text{init}}}^{P_{\text{end}}} E dP_r$ . Adapted with permission from Ref. [28]. Copyright 2016, AIP Publishing.

Below the FE  $T_c$ , that is, for  $T < T_c$ , the poled material has a remnant polarization, see Figure 1. Increasing an external field that is either non-collinear or antiparallel to the polarization may induce switching of the polarization direction if  $|E_{\text{end}}|$  exceeds the coercive field  $E_c$  of the ferroelectric hysteresis. Under adiabatic conditions, there is no heat exchange and the work loss (per unit volume),  $W_{\text{loss}}$ , causes an additional contribution to the entropy change:

$$\Delta S = W_{\text{loss}}/T_{\text{init}} \quad (15)$$

where  $T_{\text{init}}$  is the initial temperature and  $W_{\text{loss}}$  is defined as the difference (per unit volume) of total work  $W_{\text{total}}$  done on the total polarization change and the reversible work  $W_r$  done on the reversible polarization change.  $W_{\text{total}}$  and  $W_r$  are indicated by the gray and green areas in Figure 1, respectively. According to the experimental observations by Bolten et al.,<sup>[36]</sup> the reversible polarization change can be approximated by a straight line crossing the center of the hysteresis with the same slope as  $P(E)$  at the saturation polarization point as indicated by the black straight line in Figure 1. The change of entropy transferred to the vibrational degrees of freedom is thus expressed as follows:

$$\Delta S_{\text{latt}} = -\Delta S_{\text{dip}} + \frac{W_{\text{loss}}}{T_{\text{init}}} \quad (16)$$

Under reversible adiabatic modifications of the external field,  $W_{\text{loss}} = 0$ , and one regains Equation (7). Commonly,  $W_{\text{loss}} > 0$  for field application and  $W_{\text{loss}} < 0$  for field removal, resulting in an increase and a decrease of the lattice entropy, that is, heating and cooling of the material, respectively. Therefore, losses may considerably reduce the overall temperature change in case of the inverse ECE. Furthermore, the losses may differ for field application and removal, possibly resulting in a temperature drift and a reduction of the overall cooling capacity.

Equations (5) and (6) are often used for indirect determination of  $\Delta S$  and  $\Delta T$ , which can then be obtained from standard polarization measurements without the need for any additional equipment. Furthermore, no knowledge on the time evolution of the system is required, which is advantageous for some phenomenological models or Monte Carlo simulations.<sup>[17]</sup> The applicability of the indirect approach has been discussed several times, see, for example, Refs. [8, 17, 31, 37]. Its validity relies on the Maxwell relation [Eq. (3)], which implies that the free energy is a well-defined, continuous, and continuously differentiable function of  $T$  and  $E$ , that is, thermal equilibrium, and reversibility. Formally, the Maxwell relation applies to homogeneous systems. However, it has been shown that averaging over, for example, a ceramic sample yields a sufficiently well-defined thermodynamic system, and the indirect method is typically also successfully applied to ceramics and polycrystalline films. On the other hand, for cases such as the ones discussed above, where a different sample history can strongly affect the measured ECE, the application of the indirect approach can lead to particu-

larly severe errors and can create artifacts, especially for ceramics and relaxor ferroelectrics (cf. Section 4.1). Furthermore, an additional effect owing to  $W_{\text{loss}}$  is not taken into consideration in Equations (5) and (6).

### 3. Different Examples of Inverse EC Response

An electrocaloric response can in principle be observed in any dielectric material where an applied electric field induces an electric polarization. The largest conventional ECE is usually observed in ferroelectric and antiferroelectric materials, at temperatures slightly above the transition temperature between the FE (or AFE) and the paraelectric (PE) phase, that is, slightly above  $T_C$ .<sup>[7,38]</sup> Around these transitions the electric polarization typically varies strongly with temperature and field. Thus, large values for  $|\partial P/\partial T|_E$  can be obtained. In the case of a first order transition the polarization even exhibits a discontinuous jump and the latent heat of the transition can induce a giant  $\Delta T/E$ .

In the PE phase, the polarization induced by the electric field is usually parallel to the applied field and decreases with temperature, that is,  $(\partial P/\partial T)_E < 0$ . As shown in Figure 2, the system becomes more ordered when applying an electric field ( $\Delta S_{\text{dip}} < 0$ ) that leads to a conventional ECE. Thus, in the PE phase no inverse effect is expected without competing internal bias fields.<sup>[20,22]</sup>

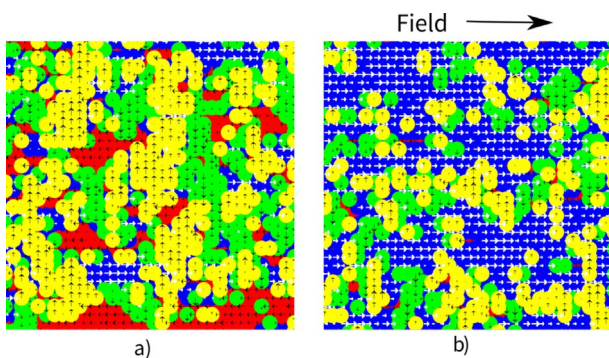


**Figure 2.** Illustration of the dipolar ordering in the paraelectric phase. Colors encode the direction of local dipoles. a) Zero field, high disorder and b) an applied field parallel to the blue dipoles results in ordering ( $\Delta S_{\text{dip}} < 0$ ), which corresponds to the conventional ECE. Adapted with permission from Ref. [40]. Copyright 2016, American Physical Society.

#### 3.1. Role of the relative direction between field and polarization

Inverse caloric effects have been reported to occur within a FE phase for certain cases where the field is applied antiparallel to the spontaneous polarization  $\mathbf{P}_s$ <sup>[18,23–28]</sup> or where the field is non-collinear to  $\mathbf{P}_s$ , in particular close to transitions between two FE phases with different polarization directions.<sup>[14,15,17–22,39]</sup> However, non-collinear or antiparallel fields are not sufficient criteria for the occurrence of an inverse EC response. In the following we discuss under which circum-

stances an inverse ECE is expected, elucidate the underlying physical mechanisms, and discuss possible ways to optimize the overall  $\Delta T$ .

#### 3.1.1. Inverse ECE through field reversal

Within the FE phase, and after initial poling, a FE material generally exhibits a finite remanent polarization. Reversal of the polarization direction is then subject to a finite hysteresis, see Figure 3a. As the width of the hysteresis increases with decreasing  $T$ , both the upper and the lower branch of the field hysteresis are states that are accessible over a large field range at low  $T$ . It should be noted that many experimental investigations using the indirect approach focus on the right part of the upper branch of the field hysteresis, that is, where  $\mathbf{P}$  is parallel to  $\mathbf{E}$  and  $E > 0$  (see Section 4.1) neglecting the possible inverse ECE discussed in the following.

Once the system is poled by applying a strong field in the positive direction, ramping the field back down to zero reduces the polarization and the system cools down (conventional ECE). However, the polarization can be reduced further if the field direction is reversed and the field is applied antiparallel to the remanent polarization. With increasing strength of the reversed field, the polarization is reduced until  $P_{\text{end}} = 0$  at the left coercive field  $E_c^{\text{left}}$ . A further increase of the negative field then results in an increase of the induced negative polarization.

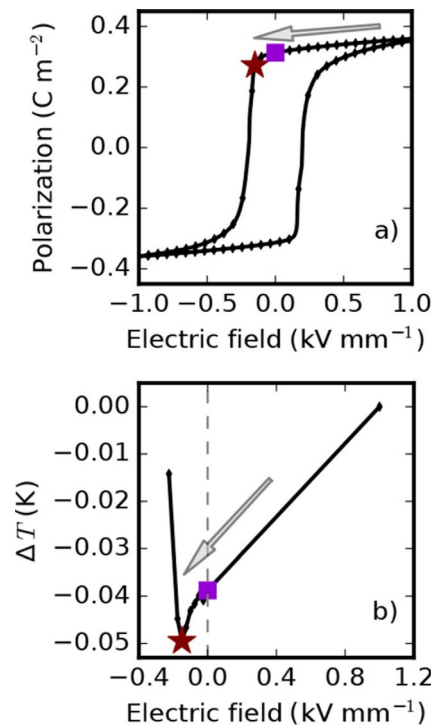


**Figure 3.** Field-dependent transition between conventional and inverse ECE under field reversal based on direct experimental measurements for  $\text{Pb}(\text{Mg}_{1/3}/\text{Nb}_{2/3})_{0.71}\text{Ti}_{0.29}\text{O}_3$  at 303 K. a) Measured field hysteresis. b) ECE depending on the final field ( $E_{\text{init}} = 1 \text{ kV mm}^{-1}$ ). The inverse ECE is found for ramping an antiparallel field down to the left shoulder of the hysteresis (brown stars). The cyan squares marks  $E_{\text{end}} = 0 \text{ kV mm}^{-1}$ . Adapted with permission from Ref. [27]. Copyright 2016, American Physical Society.

As predicted based on the simple Landau model of Equation (10),<sup>[30]</sup> the change of the dipolar entropy is related to  $\Delta(P^2) = P_{\text{end}}^2 - P_{\text{init}}^2$ , see Equation (11), and is negative if  $|P_{\text{end}}| > |P_{\text{init}}|$  and positive if  $|P_{\text{end}}| < |P_{\text{init}}|$ . The latter is the case if the reversed field strength is increased from zero up to  $|E_{\text{end}}| < |E_{\text{c}}^{\text{left}}|$ . Thus, the entropy is increased for increasing (negative) field strength, that is, an inverse ECE is obtained, which under adiabatic conditions will result in further cooling of the system. This prediction is also in agreement with Equation (4), as the increasing reversed field (negative  $dE!$ ) in combination with the negative  $(\partial P/\partial T)_E$  (for  $P > 0$ ) results in negative  $dT$ , that is, cooling. Once the polarization switches to the negative direction, that is, for  $|E_{\text{end}}| > |E_{\text{c}}^{\text{left}}|$ , the sign of  $(\partial P/\partial T)_E$  switches and a normal (positive)  $dT$  is obtained.

These predictions have been validated qualitatively by experimental findings for  $\text{Pb}(\text{Mg}_{1/3}/\text{Nb}_{2/3})_{0.71}\text{Ti}_{0.29}\text{O}_3$ .<sup>[27]</sup> Similarly, Basso et al.<sup>[26]</sup> demonstrated that the EC cooling of a FE polymer can be enhanced if a negative electric field is applied to an initially positively poled sample. Experimental and theoretical studies of adiabatic loading cycles in  $\text{Pb}(\text{Zr},\text{Ti})\text{O}_3$  also showed the occurrence of an inverse ECE under reversed electric field and indicated that a reversed electric field should also increase the overall cooling effect.<sup>[23–25]</sup> However, in contrast to the discussion so far, the maximal inverse EC response has not been observed, if the negative field is ramped exactly to the coercive field but for slightly smaller  $|E_{\text{end}}|$ , see Figure 3b. In addition, strong heating of the sample has been found for larger negative fields.

The field-induced entropy and temperature changes in the ferroelectric phase are a combination of the induced change of the dipolar entropy and the work loss of the  $P$ – $E$  loops.<sup>[28]</sup> If the reversed field induces a reduction of  $P$  without inducing actual switching, work losses are small and the inverse ECE due to the dipolar entropy change becomes appreciable. Beyond the shoulder of the hysteresis, that is, left of the brown stars in Figure 3, the irreversible losses exceed the increase of  $S_{\text{dip}}$  and the sample heats up. Meanwhile, we could also reproduce these trends using lattice-based Monte Carlo simulations<sup>[27]</sup> and ab initio-based molecular dynamics simulations for  $\text{BaTiO}_3$ .<sup>[29]</sup>

In summary, an electric field antiparallel to the remanent polarization can induce an inverse ECE in the poled ferroelectric phase. We note that this applies for positive poling (upper branch of the field hysteresis) with a negative field and for negative poling (lower branch of the field hysteresis) with positive applied field. The largest response is obtained if the field drives the system to the shoulder of the field hysteresis without ferroelectric switching. Ramping the field from positive to small negative fields can thus be utilized to enhance the overall cooling. However, a slightly too large reversed field results in large heating of the sample due to the irreversible heat losses. As illustrated in Figure 3b, one may already fully compensate the inverse cooling effect if one misses the optimal reversed field by only  $0.025 \text{ kV mm}^{-1}$ .

### 3.1.2. Inverse ECE around FE–FE transitions

As noted previously, the largest EC temperature changes are usually observed close to FE–PE transitions. In addition, many FE materials such as,  $\text{BaTiO}_3$ ,  $(\text{Ba},\text{Sr})\text{TiO}_3$ , or  $\text{Pb}(\text{Mg}_{1/3}/\text{Nb}_{2/3})\text{O}_3$ – $\text{PbTiO}_3$  (PMN–PT), exhibit multiple FE phases corresponding to different polarization directions and thus also undergo one or more first-order FE–FE phase transitions. Because the reorientation of the polarization direction at these transitions also results in a pronounced temperature dependence of the various components of  $\mathbf{P}$ , a strong ECE can also be expected in the vicinity of these transitions. There have been many studies reporting an inverse ECE at FE–FE transitions,<sup>[14,15,17,19–22,39]</sup> which we review in this section. Because the direction of spontaneous polarization differs between two FE phases, the direction of the applied field relative to both polarization directions becomes important and a pronounced anisotropy of the EC response can be expected.

One of the first studies that reports a directly measured inverse effect was presented by Peräntie et al.<sup>[14]</sup> The authors observed an inverse ECE in PMN–PT at a first-order FE–FE phase transition from a rhombohedral (or field-induced monoclinic  $M_B$ ) phase to an orthorhombic phase for a field applied along the [011] direction. The inverse ECE was explained by the latent heat associated with the field-induced phase transition. In contrast, a conventional ECE was observed at higher temperatures, where the orthorhombic phase is reached through another FE–FE transition starting from a tetragonal (or field-induced monoclinic  $M_C$ ) phase. Another study by Le Goupil et al.<sup>[15]</sup> also on PMN–PT but with the field applied along the [001] direction, reported an inverse effect obtained by both direct and indirect measurements. Here, the inverse effect was observed near the rhombohedral to tetragonal transition. Both studies thus indicate that the relative direction of applied field and the polarization directions within the two FE phases are very important.

Several theoretical studies also report an inverse EC response.<sup>[17,19–22]</sup> First-principles-based simulations for  $(\text{Ba},\text{Sr})\text{TiO}_3$ <sup>[17]</sup> predicted an inverse effect at the FE–FE transition between the orthorhombic and tetragonal phases. In this study, the non-collinearity between the applied field and the polarization was proposed as the origin for the inverse effect. When the applied field is not along the direction of the spontaneous polarization in the FE phase, the application of the field can result in disordering of the electric dipoles away from the direction of the spontaneous polarization, which increases the dipolar entropy or, equivalently, reduces thermal entropy under adiabatic conditions. However, within this picture, it remains unclear whether the applied field needs to be non-collinear to  $\mathbf{P}_s$  in the low- or high-temperature FE phase (or both of them).

A detailed theoretical study of the direction dependence of the ECE in  $\text{BaTiO}_3$  and its relation with the inverse effect was also reported by Marathe et al.<sup>[20]</sup> using first-principle-based simulations. An inverse response has been found at the FE–FE transition between the orthorhombic and tetrago-

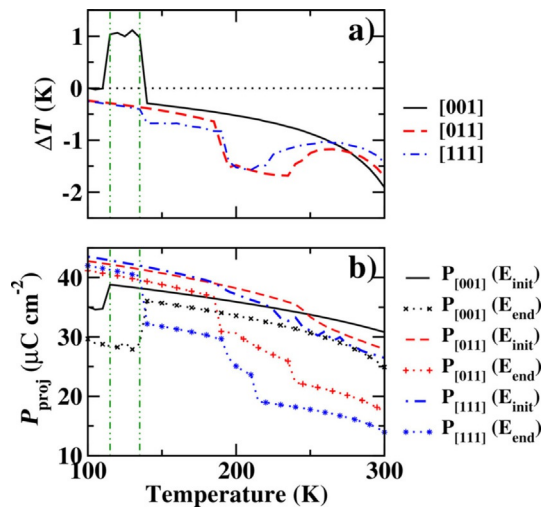


**Figure 4.** a) Adiabatic EC temperature change in BaTiO<sub>3</sub> monodomain single crystals in the temperature region around the orthorhombic to tetragonal FE–FE transition under removal of a field of  $E_{\text{init}} = 200 \text{ kVcm}^{-1}$  applied along different crystallographic directions. b) Polarization, projected along the direction of the applied field, both before and after the field-removal, for the various cases. The temperature in both (a) and (b) refers to the initial temperature, that is, the system temperature before the field-removal. The dashed vertical lines mark the region with inverse response when the applied field is along [001]. The data have been obtained using ab initio-based molecular dynamics simulations, see Ref. [20] for further details. Figure adapted with permission from Ref. [20]. Copyright 2017, American Physical Society.

nal phases for a field along [001], whereas the conventional ECE occurred for a field along [011] and [111]. The corresponding results are reproduced in Figure 4. These theoretical predictions have also been qualitatively confirmed by direct EC temperature measurements for BaTiO<sub>3</sub> single crystals, see Figure 5.<sup>[20]</sup> Furthermore, at the FE–FE transition between the rhombohedral and orthorhombic phases, the EC response is inverse for applied fields along [001] and [011] but conventional if the field is along [111].<sup>[20]</sup>

Note that in all these cases the field is non-collinear to at least one of the FE phases. The field is even non-collinear to the polarization direction of both phases for the orthorhombic–tetragonal transition and a field along [111] or the rhombohedral–orthorhombic transition and the field along [001], resulting in the conventional and inverse response, respectively.

The inverse EC response was explained by the entropy change related to the latent heat of the first order FE–FE phase transition.<sup>[20]</sup> According to the Clausius–Clapeyron equation [Eq. (14)], the sign of  $\Delta S_{\text{LH}}$  is determined by the sign of the polarization jump  $\Delta P$  across the transition. For example, in the temperature region where the inverse effect occurs for fields along [001], which is marked by dashed vertical lines in Figure 4, the system undergoes a transition from the tetragonal phase (stabilized by the applied field) to the orthorhombic phase under field removal. The polarization change at the orthorhombic to tetragonal phase transition is illustrated in Figure 4b. The polarization component projected along [001] jumps to a larger value (positive  $\Delta P$ ) when the system transforms from the orthorhombic to the tetrago-

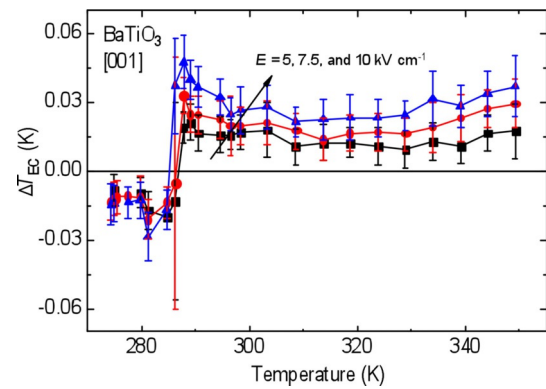


**Figure 5.** Adiabatic EC temperature change corresponding to field-application measured in a [001]-oriented BaTiO<sub>3</sub> single crystal using a custom-made adiabatic calorimeter.<sup>[20]</sup> The data represent an average over several on-off field cycles with different maximal field strengths (black:  $5 \text{ kVcm}^{-1}$ , red:  $7.5 \text{ kVcm}^{-1}$ , blue:  $10 \text{ kVcm}^{-1}$ ). One can see that around the orthorhombic–tetragonal transition temperature at  $\approx 286 \text{ K}$ , the ECE changes sign. Note that the simulation method used to obtain Figures 4 and 6 underestimates the experimental transition temperatures.  $\Delta T$  has been simulated for field removal, whereas the sign for field application is used in the experiment, that is, negative  $\Delta T$  corresponds to the inverse effect.

nal phase, for example, for increasing  $T$ . Thus, for the reverse transition occurring under field removal, the polarization jump along the field direction is negative, leading to a negative  $\Delta S_{\text{LH}}$  according to Equation (14). This means that the removal of the field in this temperature region decreases the entropy, that is, it causes an inverse ECE. Note that Equation (14) results from the generalization of Equation (5) for discontinuous  $P(T)$ , and therefore the positive jump of  $\Delta P$  along [001] observed at the orthorhombic to tetragonal transition (for increasing  $T$ ) in Figure 4 is essentially analogous to a positive  $(\partial P/\partial T)_E$  along [001].

The inverse ECE at a first-order FE–FE transition occurs exactly in those cases for which the electric field stabilizes the “higher entropy” phase that occurs at the high temperature side of the corresponding transition within the  $\mathbf{E}$ – $T$  phase diagram.<sup>[20]</sup> In such cases the applied field reduces the transition temperature for the corresponding transition and  $\Delta S_{\text{LH}}$  is positive when entering the field-stabilized “higher temperature” or “higher entropy” phase (under field application), and negative for the reversed transition (under field removal). This is also consistent with the experimental observations for PMN–PT reported in Ref. [14], where an inverse effect is observed when the field-induced orthorhombic phase is entered from the lower temperature rhombohedral (or monoclinic  $M_B$ ) phase but not from the higher temperature tetragonal (or monoclinic  $M_C$ ) phase.

The discussion above shows that, while non-collinearity between the field and the spontaneous polarization in the (initial) FE phase is of course necessary to drive the system through a transition, it is not a sufficient condition for an inverse EC response. Rather, the sign of the latent heat contribution to the entropy change, which depends on the corresponding jump of polarization along the field direction, is crucial.

A small inverse ECE can also be obtained without crossing the actual transition if the polarization along the field direction exhibits a positive  $(\partial P/\partial T)_E$  in the vicinity of the transition. In particular, this effect has been observed within a certain temperature range on the low temperature side of the orthorhombic–tetragonal transition in BaTiO<sub>3</sub> for a field along [001].<sup>[19]</sup> This example is also depicted in Figure 6,

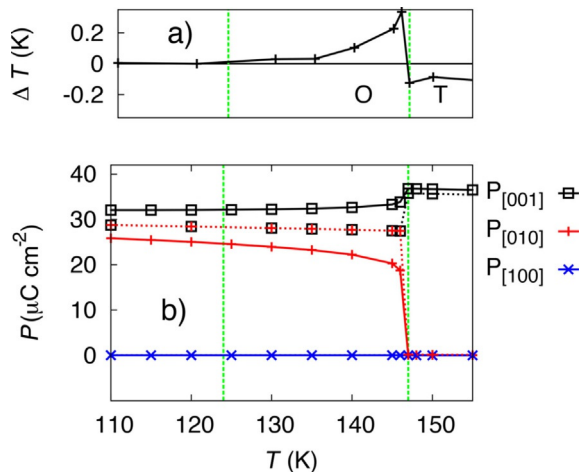


**Figure 6.** Inverse ECE close to the first-order FE–FE transition between the orthorhombic (O) and tetragonal (T) phases in BaTiO<sub>3</sub>, corresponding to removal of  $E_{[001]} = 100 \text{ kV cm}^{-1}$ . Results are obtained using first principles-based molecular dynamics simulations (see refs. [19] and [37] for details). a) Adiabatic temperature change. b) Polarization components during field-heating (solid lines) and after field-removal (dashed lines) as function of temperature. The coexistence region between T and O phases is marked by the green vertical lines.

which shows the adiabatic temperature change and the corresponding polarization components of BaTiO<sub>3</sub> for removal of a field of  $100 \text{ kV cm}^{-1}$  applied along [001] in the vicinity of the orthorhombic to tetragonal transition. These results have been obtained from first-principles-based molecular dynamics simulations similar to the ones presented in Ref. [20] and [37] using “field-heated” initial states,<sup>[19]</sup> that is, the molecular dynamics simulations are successively initialized from configurations thermalized at slightly lower temperatures with the applied field. This way, the orthorhombic phase is stabilized as the initial state throughout the whole (field-dependent) coexistence region. One observes a small inverse ECE within the coexistence region between the orthorhombic and tetragonal phases, which is indicated by vertical green lines in Figure 6. There the sign of  $(\partial P_{[001]}/\partial T)_E$  is positive. The effect becomes larger, the closer the system gets to the transition, but no first-order phase transition occurs under field removal within the coexistence region. Instead, the system undergoes a continuous rotation of the polarization direction from a field-induced monoclinic state (with  $P_{[001]} > P_{[010]} \neq 0$ ,  $P_{[100]} = 0$ ) to the zero-field orthorhombic phase ( $P_{[001]} = P_{[010]} \neq 0$ ,  $P_{[100]} = 0$ ).

Generally, close to a FE–FE transition between two different polarization directions, the system is highly polarizable by a field that is non-collinear to the initial polarization di-

rection and tends to rotate the polarization into the polarization direction of a competing FE phase.<sup>[21,22]</sup> If this competing phase corresponds to a “higher temperature” phase in the  $E$ – $T$  phase diagram, a positive  $(\partial P/\partial T)_E$  is likely to occur, creating an inverse ECE. Because no first-order phase transition occurs in this case, the corresponding inverse ECE can in principle be fully reversible. However, the resulting temperature change in BaTiO<sub>3</sub> is relatively small ( $\Delta T \approx 0.2 \text{ K}$  for a field of  $100 \text{ kV cm}^{-1}$  in Figure 6) compared to the giant EC response of  $\Delta T \approx 1 \text{ K}$  related to  $\Delta S_{\text{LH}}$  for the transition between orthorhombic and tetragonal phases.

In addition, in Ref. [20] it has been pointed out that the size of  $\Delta S_{\text{LH}}$  only depends on where in the  $E$ – $T$  phase diagram the FE–FE transition is crossed but otherwise is not directly related to the magnitude of the applied field. As long as the field is sufficient to drive the system through the transition, a “giant” EC response can be obtained for fields as small as  $20 \text{ kV cm}^{-1}$  (see Ref. [19] and [20]). Whether or not a given field is strong enough to drive the transition strongly depends on how close the system is to the transition initially. To reversibly cycle the system, the applied field needs to overcome the thermal hysteresis related to the first order phase transition,<sup>[19]</sup> which is difficult to achieve and which may result in the system getting stuck in one of the FE phases. Furthermore, complex domain patterns may form at the phase boundary with possible impact on the material properties during field cycling.<sup>[41]</sup> In both cases, the caloric response is not fully reversible in a cyclic electric field, which may be detrimental to cooling applications.

In a real material, the first-order transition usually broadens due to sample inhomogeneities, and a clear distinction between the two cases (inverse ECE with or without crossing the transition) might not always be possible. Similarly, a rather broad transition is observed in the molecular dynamics simulations for PMN–PT in Ref. [22]. However, because Equation (14) essentially represents the generalization of Equation (2) for the case of a discontinuous  $P(T)$  and both cases are related to an increase of  $P$  with temperature under constant electric field, this distinction might mostly be important for conceptual purposes. Nevertheless, if the ECE on the high temperature side of the FE–FE transition is conventional (e.g., on the high temperature side of the orthorhombic–tetragonal transition in BaTiO<sub>3</sub> for a field along [001]), then a broadening of the transition due to sample inhomogeneities will also lead to a partial compensation between normal and inverse response and therefore reduce the overall cooling of the sample. Partial compensation between the inverse response when crossing the FE–FE transition and normal response within one or both of the adjacent FE phases can also lead to non-monotonous behavior of  $\Delta T$  with the applied field strength. This has been demonstrated both in simulations<sup>[20]</sup> and in experiments.<sup>[15]</sup> Thus, the strength of the applied field needs to be optimized to obtain the largest adiabatic temperature change.

Finally, since the sign of the EC response close to a transition generally depends on the direction of the applied field, the ECE in ceramic samples can be significantly reduced due



to the random alignment of individual grains with respect to the applied field. This could lead to some grains exhibiting a conventional EC response while other grains show an inverse response leading to large temperature gradients across the grain boundaries and a strongly reduced total temperature change of the whole sample. A possible solution for this could be the use of textured samples with a preferential grain orientation.

### 3.2. Inverse ECE related to defect induced internal offsets

In acceptor-doped perovskites ( $\text{ABO}_3$ ), some A or B site ions can be substituted by ions with a lower valence, for example,  $\text{Ti}^{4+}$  ions in  $\text{BaTiO}_3$  can be substituted by  $\text{Mn}^{2+}$ . Charge neutrality is achieved through oxygen vacancies. The acceptor ions and the oxygen vacancies form defect dipoles that align with the overall polarization direction over time. This so-called aging is commonly observed in experiments.<sup>[42–47]</sup> Related to diffusion, the switching or reorientation of these defect dipoles is orders of magnitude slower than the displacive reorientation of the lattice dipoles of the host material at low and ambient temperatures. As reviewed and discussed in Ref. [48–52], such “frozen-in” defect dipoles act as an internal electrical field ( $E_d$ ) with significant influence on the dielectric hysteresis. Therefore, a strong impact on the ECE in the FE phase has to be expected, see Section 3.1.1.

The possibility to enhance and control the ECE in dielectric materials by the presence of internal dipoles was formulated in a US patent by van Vechten in 1979.<sup>[53]</sup> However, we are not aware of systematic studies on the impact of acceptor doping and aging on the EC response by other groups. Recently, Grünebohm and Nishimatsu predicted the possible appearance of the inverse ECE if defect dipoles have been equilibrated antiparallel to the external field applied in the ECE cycle (antiparallel defects), using both the direct and

indirect approach and the ab initio based effective Hamiltonian.<sup>[16]</sup> This approach was combined with lattice-based Monte Carlo simulations by Ma et al. to study the transition between conventional and inverse ECE depending on the field strength; finally, a Landau model was used for further interpretation of the impact of the field hysteresis on the inverse ECE.<sup>[29]</sup> For this, the electrostatic coupling between the defect-induced field  $E_d$  and the polarization  $-\frac{1}{2}E_d P$  was added into the Landau model of Equation (10). In the following, we review the major impact of defect dipoles in  $\text{BaTiO}_3$  aligned along [00-1] for an external field  $E$  applied along [001]. For simplicity we use the nomenclature  $P$  and  $E$  for the polarization and field component along [001].

First, we discuss the EC response within the paraelectric phase ( $T > T_C$ ). For a fixed strength of the applied field, adding antiparallel defect dipoles with increasing strength or density, the conventional ECE transforms to the inverse one, see Figure 7 a and b. Increasing the external field strength results in a transition from inverse to conventional EC response (Figure 7c). The explicit field dependence of the response for one defect configuration is illustrated in Figure 8. First, the inverse ECE increases with  $E$ . Increasing the external field further results in a reduction of the inverse ECE, the caloric response vanishes for  $E_{\text{end}} = |E_d|$ , and finally an increasing conventional ECE is found for  $E_{\text{end}} > |E_d|$ .

These trends can be understood by the opposing effect of  $E_d$  and  $E$  on the polarization. For the defect-free material, increasing the magnitude of  $E$  always results in an increase of the polarization ( $|P_{\text{init}}| < |P_{\text{end}}|$ ) and the conventional ECE (Figures 8 and 10a). However, antiparallel defects induce a finite negative polarization  $-P_d$  for  $E_{\text{init}} = 0$  (Figure 10b–d). For  $E_{\text{end}} \leq |E_d|/2$ , the external field steadily reduces the polarization ( $|P_{\text{init}}| > |P_{\text{end}}|$ ) and the system becomes more disordered after applying the electric field antiparallel to the defect dipoles as shown in Figure 9. For larger  $E_{\text{end}}$ , the polarization direction switches and  $P_{\text{end}}$  increases

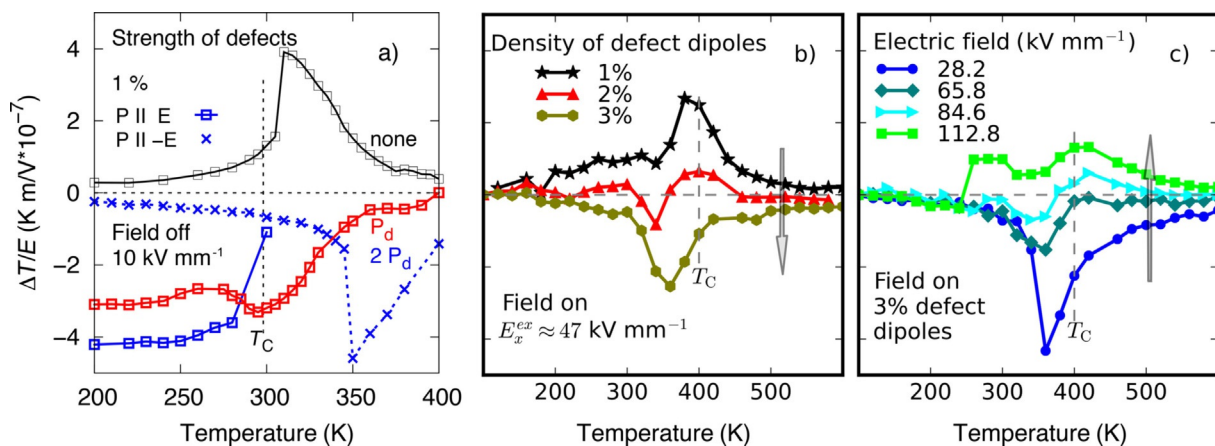


**Figure 7.** Complex  $T$ -dependency of the inverse and conventional ECE of  $\text{BaTiO}_3$  in the presence of antiparallel defect dipoles of a) different strength (black: no defects, red or blue: defects with local dipoles moment  $P_d$  or  $2P_d$ ), b) different defect densities, and c) different external field strength. a) Results based on ab initio-based molecular dynamics simulations found for field removal with reversed sign to compare with (b) and (c), cf. Ref. [16] for technical details. For crosses and squares, the initial polarization has been poled parallel to internal and external field, respectively. b, c) Data for ramping on the field taken from lattice-based Monte Carlo simulations in Ref. [40]. The initial states have been prepared by pre-poling, that is, application and removal of a positive field under isothermal conditions. Vertical lines mark  $T_C$  found by the different methods without field and defects. (b) and (c) adapted with permission from Ref. [40]. Copyright 2016, American Physical Society.

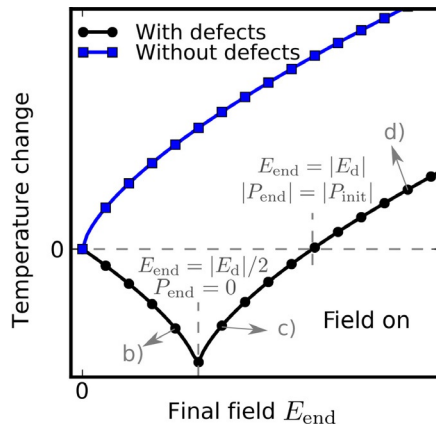


**Figure 8.**  $T > T_C$ : Schematic sketch of the field dependency of the ECE without (blue squares) and with (black dots) antiparallel defects, based on the analytic model of Ref. [29]. In the presence of defects an inverse ECE is found for  $|E_d| < E$ , which is maximal for  $E = |E_d|/2$  and  $P_{end} = 0$ . For larger fields, the conventional ECE is obtained, which increases with  $E$ , however the conventional ECE is reduced by the defect dipoles. Labels (b–d) correspond to Figure 10 (b–d), respectively.

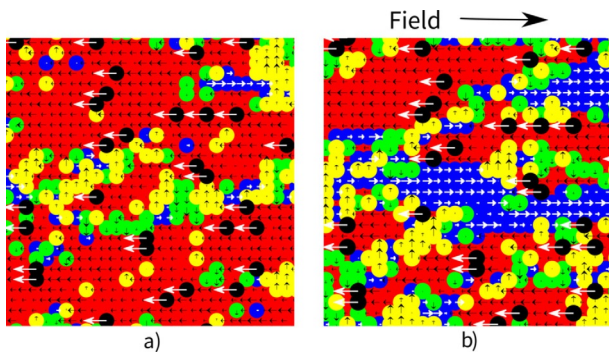


**Figure 9.** Illustration of the dipolar ordering at  $T \geq T_C$ . The black dots with white arrows represent the defect dipoles. Colors encode the direction of local dipoles (red: parallel to the defects; blue: parallel to the external field; yellow and green: perpendicular to both fields). a) Zero field: high order induced by the defect dipoles. b) an applied field antiparallel to the defect dipoles results in disordering ( $\Delta S_{dip} > 0$ ), which responds to the inverse ECE. Adapted with permission from Ref. [40]. Copyright 2016, American Physical Society.

with increasing  $|E_{end}|$ . Thus, the relative strength of both fields determines the sign and magnitude of  $\Delta T$ . It should be noted that  $E_d$ ,  $P_d$ , and thus the maximal inverse  $\Delta T$  increase with the strength and density of the defect dipoles. Hence, for sufficiently strong or dense defect dipoles both conventional and inverse ECE are of the same order of magnitude, see Figure 7. In ab initio-based simulations, we found an inverse ECE of more than 4 K. In addition, the temperature range with induced  $P$  above  $T_C$  increases with the defect dipole concentration and their strength.

Within the FE phase, the ECE in the presence of defects shows a complex dependence on  $T$  and on the sample history (previous poling conditions, field-cooling, field-heating, zero-field cooling, zero-field heating, etc.). For example, as illustrated by blue lines in Figure 7a, we found different trends for field removal for the same defect concentration. If the field is removed after field cooling, the initial polarization is aligned with  $E_d$ , resulting in a small inverse ECE that decreases systematically with decreasing  $T$  (crosses). However, for field heating both initial polarization along  $E$  and  $E_d$  are stable states up to about 300 K. If the system is initially poled along  $E$ , a large inverse ECE is induced upon removal of the field below this temperature.

These complex trends are related to the field hysteresis and its temperature dependency. As discussed for the defect-free case in Section 3.1.1, both conventional and inverse ECE can be found for  $T < T_C$ , depending on the previous poling direction and the additional contribution of work losses, if the field drives the system across the left or right coercive field. The situation is even more complex in the presence of antiparallel defects, as the center of the hysteresis is shifted towards positive values of  $E$ . For each  $E_d$ , that is, strength and density of the defect dipoles, one can define a characteristic temperature  $T'$  for which the left coercive field is zero. For  $T < T'$ , the broad thermal hysteresis results in a negative left coercive field, see Figure 11a. With increasing  $T$ , the thermal hysteresis is reduced and for  $T > T'$  the left coercive field is positive (Figure 11b and c).

It depends on temperature and external field strength, which of the following scenarios applies for each defect configuration, cf. Figure 11: case 1)  $E_c^{left} < 0$  and  $E < E_c^{right}$ ,

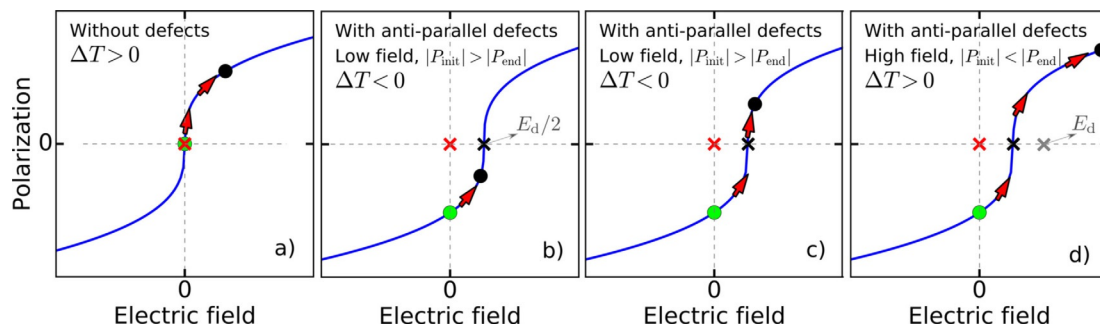


**Figure 10.**  $T > T_C$ : Schematic illustration of field induced polarization changes if the external field is ramped on from 0 to  $E_{end}$  in the presence of defect dipoles, based on the analytic model of Ref. [29]. a) No defects:  $\Delta|P(E)| > 0$  (conventional ECE for all values of  $E$ ); b)  $|E_d|/2 > E$ :  $\Delta|P(E)| < 0$  (inverse ECE) c)  $|E_d|/2 < E < |E_d|$ :  $\Delta|P(E)| < 0$  reduced by the switching of the direction (inverse ECE); and d)  $|E_d| < E$ :  $\Delta|P(E)| > 0$  reduced by the switching of the direction (conventional ECE). The lime and black dots represent the initial and final states, respectively.

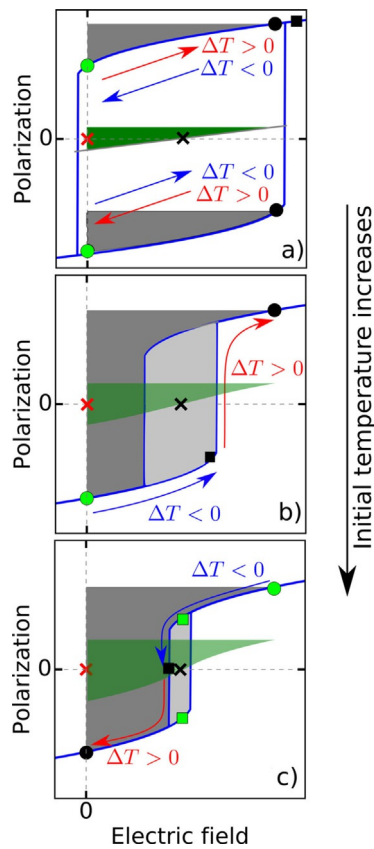


**Figure 11.**  $T < T_C$ : Schematic illustration of the temperature dependency of hysteresis, field induced polarization changes and work in the presence of defects, based on the analytic model of Ref. [29]. With increasing  $T$ , the thermal hysteresis decreases and the left and right coercive fields are shifted, resulting in a positive  $E_c^{\text{left}}$  for  $T > T'$ . Initial and final states discussed in the text are marked by lime and black symbols, respectively. Arrows illustrate the direction of the field change and are colored corresponding to the expected sign of  $\Delta T$  (red: heating, blue: cooling), see text. The total work  $W_{\text{total}}$  done by the field is highlighted in gray (dark: field removal, sum of dark and light: field application). The green areas correspond to the reversible work contribution  $W_r$  (for initial and final states marked with dots).

case 2)  $E_c^{\text{left}} < 0$  and  $E > E_c^{\text{right}}$ , case 3)  $E_c^{\text{left}} > 0$  and  $E < E_c^{\text{right}}$ , or case 4)  $E_c^{\text{left}} > 0$  and  $E > E_c^{\text{right}}$ . Here,  $E$  corresponds to  $E_{\text{init}}$  for field-application and  $E_{\text{end}}$  for field-removal.

At low temperatures for case 1, that is, between lime and black dots in Figure 11 a, either reversible conventional or inverse ECE are found, depending on the previous poling direction with respect to the applied field direction as discussed above. In these cases, the defect-induced shift of the hysteresis may enhance the response for a unipolar positive field compared to the defect free material as the slope of  $P(E)$  is larger close to the coercive field.<sup>[29]</sup> For case 2, that is, between lime dot and black square in Figure 11 a and negative poling, the polarization switches to the upper branch of the field hysteresis during the first field cycle. For further cycling or initial positive poling, a reversible conventional ECE is induced.

For strong or dense defect dipoles, that is, if the internal field exceeds  $E$ , case 3 is most relevant for a broad temperature range. As illustrated in Figure 11 b and c, the system re-

mains on the lower branch between  $E=0$  and the black or lime square for field application or field removal from the negatively poled sample. This results in the small reversible inverse ECE also found in our molecular dynamics simulations for strong defect dipoles, see blue crosses in Figure 7 a. However, if the field is removed from the positively poled sample, that is, starting from the upper branch in Figure 11 c, the polarization direction switches. As discussed above, the switching of the polarization direction reduces  $\Delta|P|$ , the sign and magnitude of which depend on the relative field strength. Furthermore, switching is related to work losses as illustrated by the difference of the dark gray area and the green area in Figure 11. These losses may induce a large inverse ECE under field removal (cf. blue squares in Figure 7 a). Here, it should be noted that this large inverse response is not accessible by a cycling field as the system remains on the lower branch of the hysteresis after the first field cycle.

For case 4 (most relevant for  $E > E_d$  and  $T \lesssim T_C$ ), the polarization direction switches for all field protocols, see lime to black circles in Figure 11 b and c. Thus, work losses contribute to the temperature change of field application and removal during subsequent field cycles. For field removal, the negative work loss is given by the difference of the dark gray area and the green area in Figure 11. For field application, the work loss is the difference between the total gray (light plus dark) area and the green area. In other words, the work loss is considerably larger for field application than its removal, particularly well below  $T_C$ .

In summary, defect dipoles aligned antiparallel to the external electrical field may reverse the sign of  $\Delta T$  (inverse ECE). In particular in the paraelectric phase, both reversible conventional and inverse ECE can be induced depending on the relative field strength. For strong or dense defect dipoles, it has been predicted that  $|\Delta T|$  of the inverse ECE may be comparable with  $|\Delta T|$  of the conventional ECE. On the one hand, this opens up the possibility to tune the overall cooling performance by the combination of conventional and inverse ECE for  $T > T_C$  simply by changing the sign of  $E$ , possibly with a much larger enhancement compared to the ideal material for  $T < T_C$  (cf. Figure 3 b). On the other hand, Figure 8 also points out a possible disadvantage of the defect-induced inverse ECE: Even a small defect-induced field in experimental samples<sup>[32,47,52]</sup> may reduce the overall conventional ECE.

Within the ferroelectric phase, also both conventional and inverse ECE can be found depending on the previous poling direction. If initial and final polarization are parallel to each other, these responses are reversible for field application and removal. Similar to the discussion in Section 3.1, the largest response is possible if the system is ramped from or to the shoulder of the hysteresis. In contrast to the ideal system discussed in Section 3.1, it is not necessary to reverse the field direction for this optimization for  $T \leq T'$ . However, this reversible inverse ECE is one order of magnitude smaller compared to the inverse response of the paraelectric phase.

The shift of the field hysteresis allows polarization switching for unipolar electrical fields. The resulting work losses may result in large inverse ECE; however, this response is different for field application and removal and furthermore depends on the previous poling conditions, which makes the integration in future devices challenging.

It should be noted that these predictions are based on different models, ranging from a simple analytic Landau model to Monte Carlo simulations and to complex ab initio-based molecular dynamics simulations with high predictive power. However, so far no atomistic simulations for actual dopants or possible relaxation of the defect dipoles with time have been conducted. Furthermore, experimental verification of the observed trends is required for a better evaluation of the technical impact.

### 3.3. Inverse ECE in antiferroelectric materials

In addition to the ferroelectric ordering discussed so far, also the entropy of other ferroic phases can be modified by an external electric field. In the following we discuss the ECE of the antiferroelectric phases appearing in some polar materials.

The characteristic behavior of antiferroelectrics can be described by the staggered polarization, which is often simplified as the polarization difference at two neighboring lattice sites. In the corresponding Kittel model the macroscopic polarization  $P$  is given as a sum of two sublattice polarizations  $P = P_1 + P_2$ .<sup>[54]</sup> At zero electric field,  $P_1 = -P_2$ , and thus  $P = 0$ , that is, the macroscopic polarization vanishes. Upon applica-

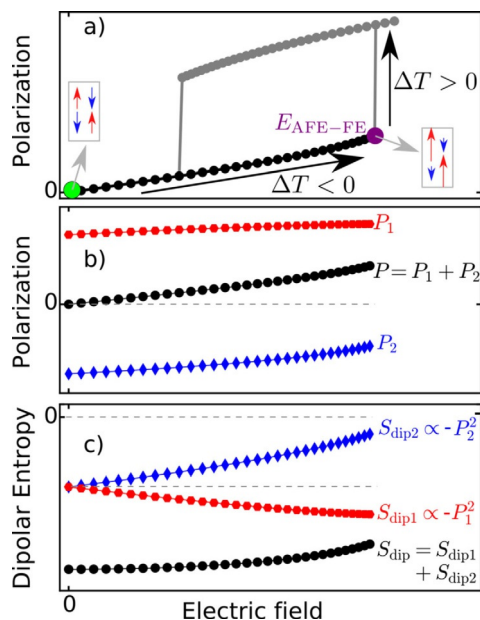


**Figure 12.** Schematic illustration of the inverse caloric response of the antiferroelectric phase based on Kittel's model.<sup>[30,54]</sup> a) For  $E < E_{AFE-FE}$ ,  $E$  induces an almost linear increase of  $P$ . The transition into the FE phase occurs at  $E_{AFE-FE}$ . b) Sublattice polarization  $P_1$  (red) and  $P_2$  (blue) for  $E < E_{AFE-FE}$ . c) Resulting field induced entropy changes of both sublattices ( $\Delta S_{dip1}$ ,  $\Delta S_{dip2}$ ) and the resulting overall inverse response ( $\Delta S_{dip}$ ).

tion of an electric field, a finite macroscopic polarization is induced, see Figure 12a. The field-induced change of the dipolar entropy  $\Delta S_{dip}$  is composed of contributions from each sublattice  $\Delta S_{dip1}$  and  $\Delta S_{dip2}$ <sup>[30]</sup> which can be calculated using Equation (11). Thus the overall dipolar entropy change of antiferroelectrics can be expressed by Equation (17)

$$\Delta S_{dip} = \Delta S_{dip1} + \Delta S_{dip2} \quad (17)$$

where  $\Delta S_{dip1} \propto -P_1^2$  and  $\Delta S_{dip2} \propto -P_2^2$ .

Figure 12b and c depicts the sublattice polarizations and the corresponding sublattice entropy as obtained by the Kittel model. In the sublattice with polarization oriented along the direction of the applied electric field, the field-induced increase of  $|P_1|$  results in a conventional entropy change ( $\Delta S_{dip1} < 0$ ). In the sublattice with polarization antiparallel to the direction of the applied electric field, the external field reduces  $|P_2|$  inducing an inverse entropy change ( $\Delta S_{dip2} > 0$ ). Globally, inverse ECE occurs since  $\Delta S_{dip2}$  overwhelms  $\Delta S_{dip1}$ . When the external field exceeds  $E_{AFE-FE}$ , it induces a phase transition to the FE phase (Figure 12a) and the latent heat of the transition will contribute to the overall ECE. Commonly, the FE phase corresponds to the “low entropy” phase stable at lower temperatures and the field induced transition contributes a conventional entropy change.

Experimentally, a very small EC effect has first been reported for the prototype antiferroelectric  $PbZrO_3$  by Lawless.<sup>[55]</sup> Pirc et al.<sup>[30]</sup> found a significant negative temperature change of  $-1$  K under a large electric field of  $100 \text{ kV cm}^{-1}$  at  $37^\circ\text{C}$  in  $PbZrO_3$  bulk ceramics. A much larger temperature drop of  $-5$  K was published by Geng et al.<sup>[13]</sup> for  $(Pb_{0.97}La_{0.02})(Zr_{0.95}Ti_{0.05})O_3$  films of 650 nm thickness deposited on a Pt(111)/Ti/SiO<sub>2</sub> substrate. Their  $P(T)$  data for different electric fields are depicted in Figure 13 and nicely show a transition from the inverse to the conventional ECE when the system is driven from the AFE into the FE phase. At high temperatures above the zero field  $T_C$  the conventional

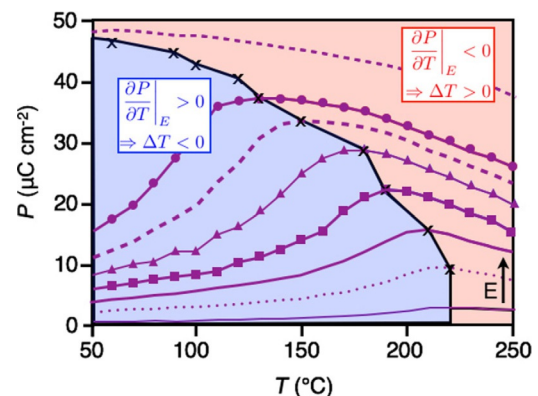


**Figure 13.** Schematic illustration of the dependency of the polarization in AFE La-doped  $Pb(Zr,Ti)O_3$  on temperature and external field strength, based on experimental data adapted from Ref. [13]. Copyright 2015, Wiley. In the blue area, where the AFE phase is present, the inverse ECE prevails, whereas in the red area the typical FE behavior showing the conventional ECE is found.

ECE already occurs as expected at low electric fields. To shed light on the basic physical mechanism that permits the inverse ECE Axelsson<sup>[59]</sup> used a 1D statistical mechanics model that only takes account of short range ordering. Based on a first-principles effective Hamiltonian approach Lisenkov and co-workers<sup>[56,57]</sup> explored the inverse effect in PbZrO<sub>3</sub>. By applying electric fields along [100], [110], and [111] directions, they found no anisotropy in the ECE, which is in contrast to the inverse ECE in ferroelectrics. They reported that the inverse and the conventional temperature changes follow different scaling laws. As already mentioned in the early experimental work by Lawless<sup>[55]</sup> for low fields and temperatures (blue area in Figure 13), the electrocaloric response of the AFE phase shows a quadratic dependence on the electric field ( $-\Delta T \propto E^2$ ) whereas conventional linear scaling ( $\Delta T \propto E$ ) characterizes the FE phase (red area in Figure 13). Based on this different scaling it was proposed, that a deviation from the AFE scaling law might indicate the presence of a minority FE phase.

It was also predicted for the prototypical AFE material PbZrO<sub>3</sub> based on ab initio simulations that depolarization and epitaxial strain modify the relative stability of the FE and AFE phase in thin films.<sup>[57,58]</sup> In particular, compressive strain systematically stabilizes the FE phase. In turn, depending on temperature, field strength, and strain both the conventional and inverse ECE can coexist.<sup>[57]</sup> The coexistence of conventional and inverse ECE in one material, which has also been found in phase-field simulations,<sup>[59]</sup> might thus explain the partly inconsistent reports on the ECE in thin films.

A combination of temperature regimes with inverse and conventional ECE was reported for a number of single-crystalline materials showing a number of phase transitions. Peräntie et al. studied (011)-PbMg<sub>1/3</sub>Nb<sub>2/3</sub>O<sub>3</sub>-0.28PbTiO<sub>3</sub> single crystals by direct measurements and identified an inverse ECE in the temperature range between 60 and 70 °C.<sup>[14]</sup> Zhuo et al.<sup>[60]</sup> recently investigated (Pb,La)(Zr,Sn,Ti)O<sub>3</sub> single crystals at different temperatures and also found a sequence of an inverse ECE owing to a temperature-driven polarization increase in the AFE phase, a conventional ECE in the FE phase, and another inverse ECE at higher temperatures due to field-induced polarization enhancement, see Section 3.1.2. Similarly, a region with negative  $\Delta T$  was identified by both direct and indirect measurements in a study on (001)-PbMg<sub>1/3</sub>Nb<sub>2/3</sub>O<sub>3</sub>-30PbTiO<sub>3</sub> single crystals.<sup>[15]</sup> This phenomenon was attributed to the formation of a reversible field-induced phase transition towards a state with a different polar direction. In lead-free ceramics Bai et al.<sup>[11]</sup> and Zheng et al.<sup>[61]</sup> predicted an inverse ECE in Na<sub>1/2</sub>Bi<sub>1/2</sub>TiO<sub>3</sub>-BaTiO<sub>3</sub> by indirect measurements and assigned it to the relaxor behavior at the ferroelectric to antiferroelectric transition. Uddin et al. predicted the inverse temperature change based on the indirect method for Na<sub>1/2</sub>Bi<sub>1/2</sub>TiO<sub>3</sub>-BaTiO<sub>3</sub> solid solutions with Ba<sub>1/2</sub>Sr<sub>1/2</sub>TiO<sub>3</sub> and explained it with the reorientation of the oxygen octahedra from the ferroelectric to antiferroelectric phase transition.<sup>[12]</sup> Jiang et al.<sup>[62]</sup> reported for (1-x)Bi<sub>1/2</sub>Nb<sub>1/2</sub>TiO<sub>3</sub>-xKNbO<sub>3</sub> that with increasing KNbO<sub>3</sub> content, the depolarization temperature shifts to lower

values and the ECE switches from inverse to conventional behavior. Recently, the coexistence of the inverse and conventional ECE has also been shown for a nanocrystalline ceramic of 0.9(Ka<sub>1/2</sub>Nb<sub>1/2</sub>)NbO<sub>3</sub>-0.1SrTiO<sub>3</sub>.<sup>[63]</sup>

As only a limited number of direct measurements were performed for antiferroelectrics experimentally,<sup>[8,24,30,64,65]</sup> it is still not clear why some materials show an inverse ECE if prepared as bulk ceramics but not as thin film and vice versa.<sup>[13]</sup> The presence of internal strain, time-dependent phenomena in relaxors, and irreversible nonpolar-polar phase transition and phase coexistence might contribute to these discrepancies (see Section 4.1). It is therefore desirable to gain a better understanding of how the AFE/FE coupling present in a given material affects the inverse ECE in the AFE phase. As we are not aware of a corresponding study in literature, we use a simple model, which is a 3D-approach similar to the 1D-model chosen by Axelsson et al.,<sup>[59]</sup> to understand these trends. Following Kittel's sublattice model, a discrete 3D-spin vector model Hamiltonian [Eq. (18)] is applied and the temperature change is calculated using a microcanonical scheme with energy daemons. The configurational energy density

$$H = - \sum_{ij} J_{ij} \mathbf{P}_i \mathbf{P}_j - \sum_i \mathbf{E} \mathbf{P}_i \quad (18)$$

consists of two parts, where the summation runs over all lattice sites  $i$ . The first part describes the interaction between two neighboring sites  $i$  and  $j$  with polarizations  $P_i$  and  $P_j$ . The interaction strength is controlled by the coupling-parameters  $J_{ij}$  that are taken from a Gaussian distributed around a mean value  $J_0$  with a standard deviation of  $\Delta J$ . The second part is a local part that consists of the interaction of the polarization with the external field  $\mathbf{E}$  that is applied in  $z$  direction. The number of directions for all polarizations is limited to six ( $\pm x \pm y \pm z$ ) and the length of the polarization vectors is kept fixed at one length and only the direction is allowed to change. If  $J_{ij}$  is positive, the polarization of cells tend to align parallel and thus the material behaves like a ferroelectric material. If  $J_{ij}$  is negative the material becomes antiferroelectric.

While keeping  $\Delta J = 1$  constant, we changed the mean coupling parameter stepwise from  $-3$  (AFE) through  $0$  (AFE/FE) to  $+3$  (FE) and examined the change in the ECE. Figure 14a shows contour plots for five different electric fields in which the change in temperature is shown in different colors. Blue indicates no or small temperature change, red and yellow a large change, and green a negative change. The horizontal dotted lines at  $J_0 = -2$  and  $J_0 = -0.5$  show the positions of the curves from Figure 14b and c. In agreement to the literature described before, an inverse ECE is observed for small electric fields and low temperatures if there is only AFE coupling present ( $J_0 < -1$ ,  $\Delta J = 1$ ). When the electric field change increases ( $E > 40$ ) or if the temperature is increased ( $T > 7$ ), the negative effect vanishes because the FE phase is induced or the system becomes paraelectric. The antiferroelectric system experiences a positive (or conven-

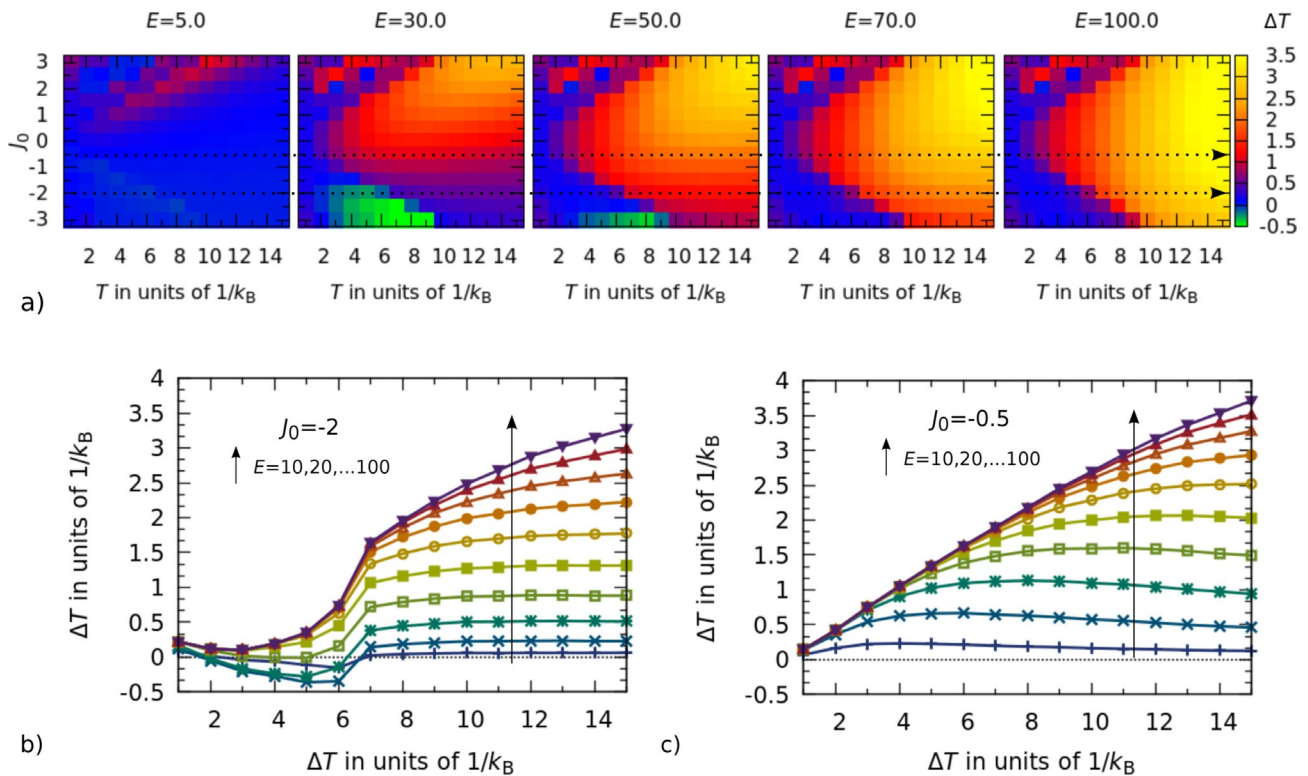


**Figure 14.** Electrocaloric temperature change after the onset of an electrical field based on the spin lattice model in Equation (18). All numbers are given in reduced units. The contour plots in (a) show temperature variations for different coupling parameters  $J_0$  varying from  $-3$  (AFE) to  $3$  (FE) at different electric fields and initial temperatures. The Gaussian width  $\Delta J = 1$  of the coupling parameters is kept constant for all calculations. The data shown in (b) and (c) correspond to the horizontal lines at  $J_0 = -2$  and  $-0.5$ .

tional) ECE only for higher electric fields or temperatures (Figure 14b). For the mixed AFE/FE case shown in Figure 14c the temperature change is always positive.

We can thus conclude that the presence of some AFE disorder in a predominantly FE-ordered material cannot induce an inverse ECE. One rather needs a dominantly AFE ordered state to obtain a significant inverse ECE. The transition between inverse and conventional ECE with increasing field strength or reduced AF coupling is similar to the discussion on pinned defect dipoles in the previous section. Likewise, defect dipoles can only induce an inverse ECE if the internal bias field exceeds the external field.

#### 4. Discussion

In the previous two sections, we have discussed the basic thermodynamics relevant for the (inverse) EC effect and described different cases where the inverse EC response has been studied in detail. In this section, we describe wider aspects related to the inverse EC response such as possible “misinterpretation” related to the indirect measurements. We then briefly describe analogous inverse effects observed in magnetocaloric and elastocaloric materials. We also discuss how this effect can be used for practical applications through a refrigeration cycle that combines conventional and inverse effects and describe the possible drawbacks that should be avoided to design efficient devices.

#### 4.1. Artifacts of the indirect method

In addition to the different mechanisms giving rise to the inverse EC effect discussed in Section 3, the prediction of an inverse ECE from experimental results can also be based on artifacts of the indirect method, see Section 2. First, suitable measurements of the pyroelectric coefficient  $(\partial P/\partial T)_E$  are necessary.<sup>[69]</sup> For example, violation of the isostress and iso-field conditions, especially in the case of thin films clamped to a substrate, may result in non-intrinsic contributions to the pyroelectric effect and in extremely large deviation between measured electrocaloric and pyroelectric coefficients.<sup>[70]</sup>

To evaluate  $(\partial P/\partial T)_E$  from experimental measurements,  $P(T)$  curves are usually extracted from  $P(E)$  measurements at different  $T$ , and are then fitted by a polynomial of high order (fourth or sixth) within a small temperature range. If the resulting  $P(T)$  curves are not smooth enough, for example, because of too large temperature intervals, this may give rise to large discrepancies, see also Ref. [8]. Typically the  $P(T)$  curves for different values of  $E$  are estimated from the upper branch of the polarization–electric field hysteresis loops measured at different temperatures. Thus, the possible appearance of the inverse ECE for small fields sampling the lower branch and possible field-induced switching events (Section 3.1.1) are not considered.

Furthermore, the indirect approach may result in the artificial inversion of the electrocaloric effect in certain tempera-

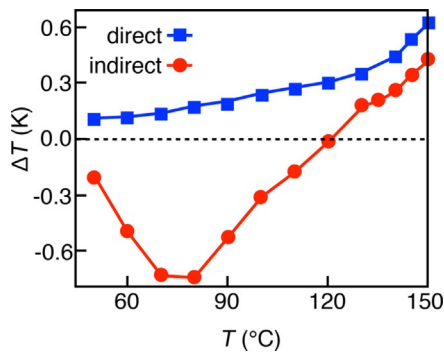


**Figure 15.** Example for the artificial prediction of an inverse ECE by the indirect method in NBT-18KBT ( $0.92\text{Na}_{0.5}\text{Bi}_{0.5}\text{TiO}_3-0.18\text{K}_{0.5}\text{Bi}_{0.5}\text{O}_3$ ) unpoled ceramics. A comparison between the direct and indirect ECE versus temperature measured for  $22\text{ kV cm}^{-1}$  is shown. Figure adapted with permission from Ref. [66]. Copyright 2015, AIP Publishing.

ture or electric field intervals, see Figure 15. Such inversion is observed when unsaturated hysteresis loops are used for the analysis. At low temperatures the coercive field is large and for many unpoled ceramics, for example, after zero-field cooling, the applied electric field is not strong enough to switch most of the domains. This results in a reduced polarization in the entire  $P(E)$  loop, see Figure 16a. For increasing

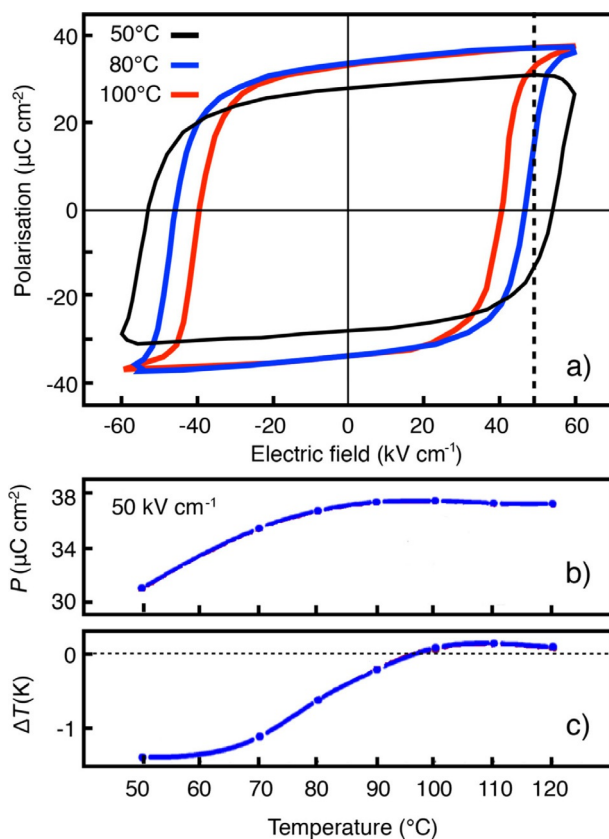


**Figure 16.** Illustration of the failure of the indirect method for NBT ceramics. a)  $P(E)$  loops of NBT ceramics measured at different temperatures, b) the extracted temperature dependences of polarization, and c) the estimated electrocaloric temperature change. Figure adapted with permission from Ref. [67]. Copyright 2014, Elsevier.

temperature the coercive field value decreases and more effective polarization switching becomes possible, for example,  $P(E)$  increases. Correspondingly, the field induced polarization will increase with temperature, and the resulting positive sign of  $(\partial P/\partial T)_E$  will imply the inverse ECE (Figure 16b,c). Examples of analysis of such unsaturated hysteresis loops resulting in growing  $P(T)$  and inverse ECE were found in  $\text{Na}_{0.5}\text{Bi}_{0.5}\text{TiO}_3$ ,<sup>[11,67]</sup> Sr and Nb co-doped  $\text{Pb}(\text{Zr},\text{Ti})\text{O}_3$ ,<sup>[71]</sup>  $\text{K}_{0.5}\text{Na}_{0.5}\text{NbO}_3-0.1\text{SrTiO}_3$ ,<sup>[63]</sup> and  $\text{Ba}(\text{Zr},\text{Ti})\text{O}_3(\text{Ba},\text{Ca})\text{-TiO}_3$ <sup>[72,73]</sup> (all ceramics).

In certain cases, the sign change is not related to any phase transition. While in  $(1-x)\text{Ba}(\text{Zr}_{0.2}\text{Ti}_{0.8})\text{O}_3-x(\text{Ba}_{0.7}\text{Ca}_{0.3})\text{TiO}_3$ <sup>[72]</sup> and  $(\text{Ba}_{0.9}\text{Ca}_{0.1})(\text{Ti}_{0.5}\text{Zr}_{0.5})\text{O}_3$ <sup>[73]</sup> ceramics the inverse ECE was related to the tetragonal-rhombohedral and orthorhombic-tetragonal transition, respectively, it was actually observed at temperatures several tens of degree above the corresponding transition temperatures. For some similar materials the comparison between the directly and indirectly measured ECE shows that the negative sign of the latter is an artifact.<sup>[31,66,74]</sup> Therefore, for NBT-18KBT ( $0.92\text{Na}_{0.5}\text{Bi}_{0.5}\text{TiO}_3-0.18\text{K}_{0.5}\text{Bi}_{0.5}\text{O}_3$ ) ceramics, Le Goupil et al.<sup>[66]</sup> found that direct measurements yield a positive ECE in the full studied temperature range while indirect estimations result in an inverse ECE at low temperatures. The authors assigned this discrepancy to be a result of the combination of the hysteresis loops not being fully saturated at the maximal field used ( $22\text{ kV cm}^{-1}$ ) and the decrease of the coercive field with increasing temperature, which leads to an increase of the induced polarization with temperature. Similarly, Birks et al.<sup>[31]</sup> found that for unpoled NBT ceramics the indirectly estimated ECE changes the sign from negative to positive on heating whereas the directly measured effect remains positive in the full temperature range. They attributed this discrepancy to an increased resistance of polarization reorientation to the change in the electric field when the temperature is lowered. The low-temperature state of unpoled NBT has relaxor character, with the polar structure consisting of polar nanoregions (PNR) with sizes of a few nanometers, with dipole moments frozen below the freezing temperature. At low temperatures these PNRs are difficult to reorient using an applied electric field. Upon heating, their reorientation becomes easier and the polarization measured from hysteresis loops grows.

More effective switching may be achieved by using lower frequencies for  $P(E)$  hysteresis loop measurements (also this will approach the experimental conditions of a typical direct EC experiment when a pulse electric field is applied) and/or by increasing the strength of the electric field. For example, in the case of relaxor  $0.9\text{PMN}-0.1\text{PT}$  films a good agreement between the indirect and direct measurements (in both cases the ECE was positive) was observed at large electric fields ( $>30\text{ kV cm}^{-1}$ ), which transfers the PNR state to the poled ferroelectric state.<sup>[75]</sup>

A completely erroneous assignment of the inverse ECE can arise in more complex cases and in particular for irreversible contributions falsely assigned to the caloric effect. We here show an example of a two-phase material, poly(vinyl-

dene fluoride-co-trifluoroethylene) (PVDF-TrFE), with embedded micrometer-sized BaTiO<sub>3</sub> particles. The sample was poled by corona poling before the deposition of the electrodes. Afterwards,  $P(E)$  loops were recorded at different temperatures. During heating, the fit of the polarization versus temperature plot yields a smooth decline and a polynomial fit of 6th order will yield an apparently reliable ECE of 2.4 K, see Figure 17a and c. Upon cooling it is clear that the system does not go back to its original state but remains depolarized (Figure 17b). The field applied by the  $P(E)$  measurements results only in a partial polarization of the film. If the cooling cycle is fitted by a 6th order polynomial, a strong inverse ECE appears (Figure 17d). This is a completely incorrect interpretation because the sample has partly depolarized. Fitting the entire span of temperature cooling yields a completely arbitrary fitting function. If measured at each temperature separately, the true ECE will be positive but strongly reduced because of the depolarization of the sample.

In summary, in polycrystalline relaxor or ferroelectric ceramics, the electric fields applied by standard polarization hysteresis measurements might be insufficient to fully pole the ceramics at low temperatures (in particular for high frequencies). On heating, the coercive field decreases, which results in the growth of the switchable polarization, and therefore a spurious inverse electrocaloric effect is found by the indirect method. Possible indications for these artifacts are temperature- or field-frequency-dependent transitions between conventional and inverse ECE as well as simple depolarization.

#### 4.2. Analogies to the inverse magnetocaloric, barocaloric, and elastocaloric effects

In addition to the electrocaloric effect, there exist other ferroic cooling effects that can be described by similar Maxwell relations to Equations (2) and (4).<sup>[2,7,34,76,77]</sup> For these responses both conventional and inverse responses were also found depending on the choice of the material, the temperature ranges, and direction and size of the external stimuli. In the following, we discuss some analogies to the ECE, but a general review is out of our scope.

The magnetocaloric effect is related to  $(\partial M/\partial T)|_H$ , with  $H$  and  $M$  the components of the magnetic field and the magnetization along the field direction.<sup>[34,78–83]</sup> Commonly, a conventional magnetocaloric effect is observed in the paramagnetic phase and at the ferromagnetic to paramagnetic phase transition, analogous to the discussion for ferroelectrics in Section 3. In the saturated ferromagnetic phase, the response is conventional and in principle also an inverse magnetocaloric effect is to be expected for antiparallel fields, analogous to the discussion in Section 3.1.1. However, the field-induced changes of  $M$  in the saturated state are insignificant and thus the corresponding small conventional and inverse responses are not of technical relevance.

Some magnetic materials such as Ni–Mn-based Heusler alloys undergo a coupled structural–magnetic phase transition with  $(\partial M/\partial T)|_H > 0$  (e.g., between ferromagnetic and antiferromagnetic phase).<sup>[34,78–82]</sup> In these cases, a giant inverse calorific response can be induced as the external field stabilizes the “high entropy” phase<sup>[34,78–83]</sup> analogous to the discus-

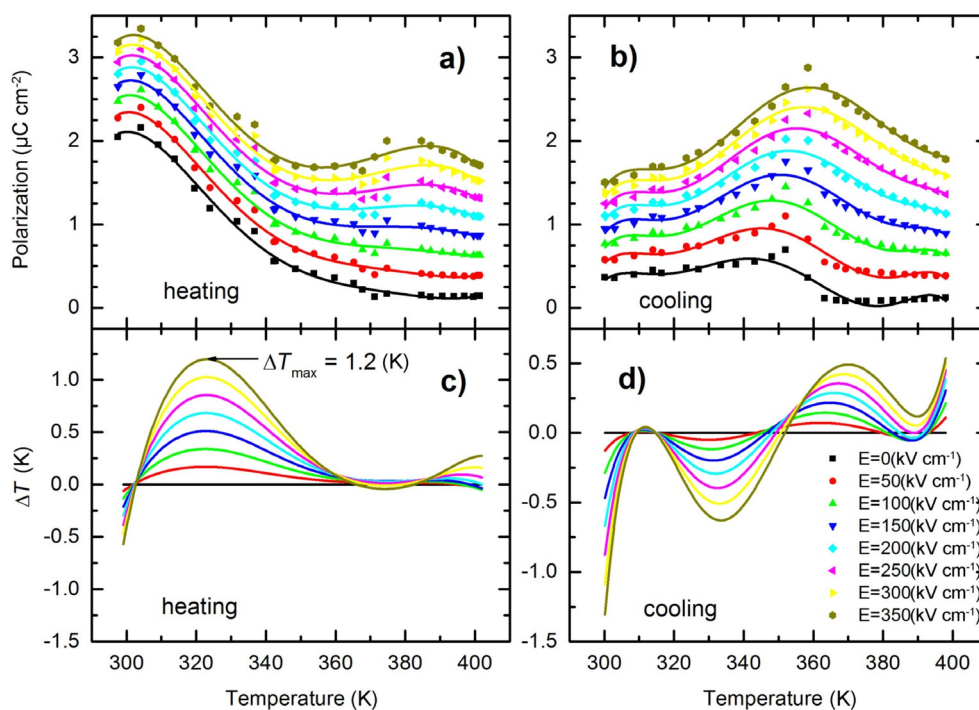


**Figure 17.** Erroneous assignment of inverse ECE in a partly depolarizing sample of PVDF-TrFe 10% BaTiO<sub>3</sub>.<sup>[68]</sup> After poling, the polarization in dependency of temperature and external field strength has been measured during a) heating and b) cooling of the sample. c, d) ECE calculated from a 6th order polynomial fit using Equation (6).



sion for ferroelectrics in Section 3.1.2. Despite this analogy, there are important differences between the responses of FE and magnetic materials. In the FE case, the ECE at the FE–FE transitions is anisotropic and even the sign of the response depends on the field direction. In contrast, the inverse magnetocaloric effect is related to a transition between different magnetic orderings, for example, ferro- and antiferromagnetic phases. Thus, one can expect that an external field always induces the inverse magnetocaloric effect for all possible relative alignments of field and magnetization. An even closer analogy could be drawn between the antiferromagnetic–ferromagnetic transition and a transition between a low-temperature AFE phase and a high-temperature FE phase. Indeed, an inverse ECE has been predicted at a corresponding phase transition for polycrystals of  $\text{Pb}_{0.99}\text{Nb}_{0.02}(\text{Zr}_{0.85}\text{Sn}_{0.15}\text{Ti}_{0.02})_{0.98}\text{O}_3$  using the indirect method by Xu et al.<sup>[84]</sup>

The inverse ECE in polar materials shows an important additional difference compared to the inverse response at the magnetostructural phase transition. In the magnetic case, the external field couples to the magnetic degrees of freedom while the latent heat is related to the transition of the structural degrees of freedom. Gottschall et al.<sup>[85]</sup> highlighted the resulting dilemma for the magneto–structural transition: The entropy changes of the magnetic degrees of freedom and of the structural ones have opposite signs. In the FE/AFE cases the polarization is part of the lattice degrees of freedom and, as shown in Section 3.1.2, the latent heat of the transition and the continuous polarization change can also add up.

In addition to external electrical or magnetic fields, elastic stimuli may also induce structural–ferroic phase transitions and induce large caloric responses. First the barocaloric effect is related to hydrostatic pressure  $\sum_{i=j}\sigma_{ij} = -p$ , which couples to the fractional volume change  $V' = \Delta V V^{-1}$  ( $F = U - TS - \mathbf{E} \cdot \mathbf{P} + pV'$ ). Inverse barocaloric effects were reported for various materials.<sup>[86–92]</sup> In particular, as measured directly in Ref. [90],  $\text{BaTiO}_3$  ceramics show an inverse barocaloric effect at the T–O and T–C phase transitions. At both phase boundaries, the high-temperature phase with higher entropy has a smaller volume. Thus, by applying an external pressure one can induce a transition to the “high-entropy” phase and the entropy increases with the latent heat of the transition in analogy to the discussion of the inverse ECE in Section 3.1.2. Furthermore, in analogy to the discussion for the ECE, it was reported that the broad thermal hysteresis of the T–O transition may induce an irreversible response whereas reversible temperature changes were found at the T–C transition.

One important difference between the ECE and the barocaloric effect is the isotropic character of hydrostatic pressure. Thus, in contrast to the ECE at FE–FE transitions, each pressure-induced phase transition either always shows the conventional or the inverse response.

Uniaxial stress is a tensor quantity and an anisotropic caloric response is likely at FE–FE transitions, analogous to the discussion of the ECE in Section 3.1.2. The resulting elastocaloric effect is related to  $(\partial\eta/\partial T)|_{\sigma}$  with  $\sigma$  and  $\eta$  the components of the stress and strain tensors along the direction of

an uniaxial stress  $\sigma_i$ . For example, one would expect a stabilization of the T or O phase by tensile stress along [001] and [011], respectively. We are not aware of a systematic study on the stress-induced phase transition in ferroelectrics for different field directions. Lisenko and Ponomareva reported the stabilization of the T phase by tensile stress along [001] resulting in a large conventional elastocaloric effect above  $T_C$  of the T–C transition for  $(\text{Ba,Sr})\text{TiO}_3$  by a stress-induced first-order phase transition.<sup>[93]</sup> The same trends were found for  $\text{BaTiO}_3$  by means of Landau theory in Ref. [94]. Similar trends occur for AFE materials. For instance, a conventional ECE was reported for a stabilization of the AFE phase by compressive stress along [010] for  $\text{PbZrO}_3$ .<sup>[95]</sup>

Inverse elastocaloric effects were reported in Refs. [98 and 99] in several materials including ferroelectrics and antiferroelectrics. Phenomenological calculations on  $\text{BaTiO}_3$ -based capacitors and thin films by Liu et al.<sup>[99,100]</sup> yield inverse elastocaloric responses under compressive stress (below certain critical magnitude) applied along [001] to the tetragonal phase. The mechanism resembles the discussed inverse ECE induced by the reversed electric fields in Section 3.1.1. The authors proposed the caloric cycle concept of combining the tensile and appropriate compressive stress to take advantage of conventional and inverse elastocaloric effect similar to that explained in Section 4.3.<sup>[99]</sup> Furthermore, they reported that the elastocaloric response depends crucially on epitaxial strain.<sup>[100]</sup>

Although one could expect an inverse response at FE–FE transitions, for example, the T–O transition of  $\text{BaTiO}_3$ , this needs verification by future work. For  $\text{PbZrO}_3$  it was predicted that tensile stress along [010] may induce the antiferroelectric to paraelectric phase transition resulting in an inverse elastocaloric response.<sup>[95]</sup>

In ferroelectric and antiferroelectric materials, the strong coupling of the structural and polar degrees of freedom thus allows large electro-, baro-, and elastocaloric responses at the same phase transitions. On the one hand this facilitates enhancement of the overall caloric response or adjustment of the operation range by the combination of multiple stimuli or the choice of static elastic and electric boundary conditions.<sup>[94,100–106]</sup> On the other hand at all FE–FE transitions it depends on the choice of the stimulus and additionally on its direction (for the ECE and the elastocaloric response) and its sign whether the system shows a conventional or inverse response. Therefore, electro-, elasto-, and barocaloric responses may also compensate each other. This signifies that more studies on underlying mechanisms are needed to achieve practical multicaloric effects.<sup>[107,108]</sup>

### 4.3. Benefits and possible issues

As mentioned in Section 1, several suggestions have been made to combine inverse and conventional ECE to achieve larger overall temperature changes and improved cooling. Figure 18 illustrates an example of the possible benefits of the combination of conventional and inverse ECE through field reversal or the additional application of non-collinear

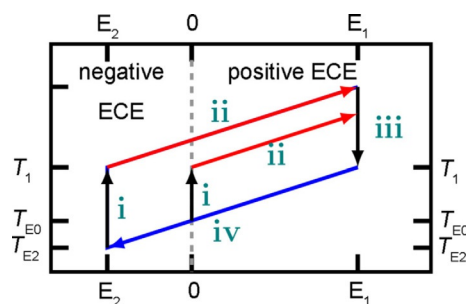


**Figure 18.** Example for the combination of conventional and inverse ECE by reversed or non-collinear field to enhance the overall temperature span  $\Delta T$  in an EC cycle. The inner cycle utilizes the conventional ECE (ramping the field between 0 and  $E_1$ ), while the conventional and inverse ECE are combined in the outer cycle (applying a second field  $E_2$ ) enhancing the  $\Delta T$ : i: isothermal heat absorption, ii: adiabatic heating, iii: isothermal heat release, and iv: adiabatic cooling. Adapted from Ref. [27] with permission. Copyright 2016, American Physical Society.

field. The inner cycle illustrates the cooling by means of the conventional ECE and a unipolar field  $E_1$ . The overall temperature change can be enhanced, if the field is not simply removed but ramped to  $E_2$ , which is either antiparallel or non-collinear to  $E_1$ , see the outer cycle. We note that one can also enhance  $\Delta T$  by simply increasing the strength of  $E_1$ . However, the combination of inverse and conventional ECE allows to obtain the same  $\Delta T$  for a smaller maximal magnitude of the applied field. This is a promising alternative as one can reduce Joule heating and avoid ferroelectric breakdown.

As seen in all examples discussed throughout this article, inverse and conventional effects occur in the same systems and within field and temperature regions that are in most cases very similar to each other. Thus, only a small change in temperature or an applied field that is slightly too high can switch the EC response from inverse to conventional and vice versa. To realize combined EC cooling cycles, such as the one depicted in Figure 18, and combine inverse and conventional effect in an optimal way, it is therefore crucial to have good control of the applied field and the main characteristics of the active material (i.e., homogeneous and sharp phase transition temperatures, grain orientation, defect structure etc.).

To utilize the inverse ECE at first-order transitions, one has to overcome potential problems with irreversibilities and the thermal hysteresis. In particular irreversible changes of the domain structure and the sticking of the system or parts of it in the coexistence range may result in the degeneration of the caloric response and an irreversible heating of the sample. These aspects need further investigation by direct determinations of the ECE in cycling electrical fields. Also, if the transition is very sharp in temperature, this can limit the temperature range available for efficient cooling. The possibility to also work at FE–FE transitions, and not just above the FE–PE transition temperature, provides further flexibility in choosing suitable materials for future applications. Furthermore, large adiabatic temperature changes at

the transitions can in principle be achieved using relatively small fields through the latent heat contribution [Eq. (14)]. For such fields, inverse and conventional ECE at the transitions can be of the same order of magnitude.

Defect engineering in a ferroelectric material provides an additional promising route to tune the inverse EC response, particularly above  $T_C$ . This concept asks for experimental verification. In the FE phases, an enhancement of the inverse ECE by defects is also possible; however, this comes along with the issue of irreversibilities, as discussed in Section 3.2. In particular, field application and removal may result in different work losses and thus irreversible temperature changes. Most likely these irreversibilities are negligible without switching of the polarization or for slim hysteresis, for example, close to phase transitions or in case of relaxors. Moreover, defect dipoles may switch with time, trying to follow the polarization of the host matrix due to electrostatic coupling. The impact of switching defect dipoles on inverse ECE and the ECE cycle remains a challenging topic.

For both the inverse ECE at FE–FE transitions and above  $T_C$  for defect doped materials, one can furthermore think of tuning the temperature range with maximal inverse response by the use of solid solutions such as Ba(Zr,Ti)O<sub>3</sub> or Ba(Sr,Ti)O<sub>3</sub> to obtain large inverse responses at lower temperatures.<sup>[17,109–113]</sup> Strain engineering may also be used for this purpose.<sup>[103–106,114]</sup>

Another possibility to stabilize large inverse responses below  $T_C$  is the appearance of the antiferroelectric phase in some materials. However, in this case one may not be able to switch between conventional and inverse ECE by a simple rotation or reversal of the field direction due to the reported isotropic character of the inverse response. In addition, the field-induced transition into the ferroelectric “low entropy” phase has to be avoided.

Because an EC device must be driven cyclically, fatigue can be an issue. Unipolar cycling has almost no influence.<sup>[115]</sup> In addition, small negative fields are not critical as studies of partially negative fields in cyclic loading have shown. Thus, as long as the inverse ECE is legitimately applicable for the different cases discussed above, fatigue should not be a major issue. Only very high cycle numbers may ultimately yield problems.

However, at the very moment when irreversible switching sets in at negative fields for a bipolar field cycling, the significant fatigue damage also starts.<sup>[116]</sup> For ferroelectric thick films and bulk materials, ionic drift is one of the major reasons leading to fatigue. Due to the strong electric fields encountered at domain walls, ionic drift is actually stronger under bipolar loading of a ferroelectric than under unipolar loading.<sup>[115,117]</sup> The resulting internal fields then shift the bipolar hysteresis.<sup>[118]</sup> As discussed in Section 3.2, depending on the direction and magnitude of the shift, both conventional and inverse ECE can either be enhanced or reduced by such bias fields. Furthermore, these fields act very locally, and individual grains in ceramics encounter increasingly different field environments and ultimately strain differences in adjacent grains may yield microcracking.<sup>[119]</sup>

## 5. Summary and Outlook

From the discussion in the preceding sections, it becomes clear that the inverse electrocaloric effect (ECE) is neither a pure artifact nor a small absurdity. There are various materials giving rise to an actual inverse ECE, the magnitude of which is comparable to the conventional ECE. In fact all ferroelectrics (FE) can potentially exhibit an inverse ECE response for certain field protocols.<sup>[23,24,26,27]</sup> Most reports of inverse EC response can be assigned to one of the following categories: 1) Ferroelectrics with an electric field applied antiparallel to the remanent polarization within the FE phase. 2) Systems with FE–FE phase transitions, where the applied field can induce a transition to a higher-entropy phase for which the spontaneous polarization is oriented more favorably with respect to the applied field or at least rotates the polarization partially towards this direction. 3) Antiferroelectrics (AFE) for field strength below the critical field strength of the AFE–FE transition. 4) Acceptor-doped aged FE materials with internal bias fields antiparallel to the applied field. In general, inverse effects are likely for all systems with imprint fields.

We note that there have been a few reports on inverse ECE that do not directly fall in these categories. For instance, reduction or rotation of polarization by mechanical stress or surface effect can lead to an inverse ECE.<sup>[59]</sup> Furthermore, based on phase-field simulation, Li et al. reported a local inverse ECE at 180° domain walls.<sup>[18]</sup> They claimed that this inverse ECE is due to the decrease of local polarization when the direction of the applied electric field is opposite to the dipole direction of the domain pattern (see discussion in Section. 3.1.1).

An inverse ECE was reported also for some relaxor systems.<sup>[14]</sup> However, it has the same origin as for conventional ferroelectrics when the applied field stabilizes the high-entropy phase and is not related to a particular relaxor character of these materials.

It appears that in all these cases the inverse ECE is related to the presence of competing phases or other sorts of competing states, for example, oppositely poled remanent states or domain configurations, different FE phases, competition between the dipolar field owing to polar defect complexes and the externally applied field, or between the AFE and a homogeneously polarized phase. The applied field then destabilizes the initial order in favor of the competing one.

A good understanding of the circumstances under which inverse EC effects can occur is not only desirable for enhancement of the overall ECE but also for avoiding unintentional superposition of conventional and inverse effects. In particular, small bias fields in the presence of defects or by fatigue may reduce the conventional response.

Furthermore, the experimentally observed inverse ECE in ceramics and relaxors may be an artifact of the indirect method as discussed in Section 4.1. The appearance of a temperature or frequency dependent transition between conventional and inverse ECE away from phase transitions and fer-

roelectric switching as well as unsaturated polarization loops, are warnings for this artifact.

We hope that this extensive Review on the inverse electrocaloric effect will encourage further studies on this important aspect and facilitate the further development of devices based on the ECE.

## Acknowledgements

*Financial support has been guaranteed by the Deutsche Forschungsgemeinschaft via the SPP 1599 (projects: GR 4792/1-2, XU 121/1-2, AL 578/16-2, LU 729/15, and by the Swiss National Science Foundation under project code 200021E-162297. Computational resources were provided by the Center for Computational Science and Simulation (CCSS), University of Duisburg-Essen, and Competence Center of High Performance Computing in Hesse (HPC Hessen). The authors thank Franziska Scheibel and Mehmet Acet for fruitful discussions on the magnetocaloric effect and Maksim Olegovic Karabasov for helping with Figure 17.*

## Conflict of interest

*The authors declare no conflict of interest.*

**Keywords:** antiferroelectrics • defect engineering • disorder • ferroelectrics • electrocaloric effects

- [1] A. S. Mischenko, Q. Zhang, J. F. Scott, R. W. Whatmore, N. D. Mathur, *Science* **2006**, *311*, 1270–1271.
- [2] S. Fähler, U. K. Röbber, O. Kastner, J. Eckert, G. Eggeler, H. Emmerich, P. Entel, S. Müller, E. Quandt, K. Albe, *Adv. Eng. Mater.* **2012**, *14*, 10.
- [3] I. Takeuchi, K. Sandeman, *Phys. Today* **2015**, *68*, 48–54.
- [4] J. F. Scott, *Annu. Rev. Mater. Res.* **2011**, *41*, 229.
- [5] M. Valant, *Prog. Mater. Sci.* **2012**, *57*, 980.
- [6] *Electrocaloric Materials—New Generation of Coolers* (Eds.: T. Correia, Q. Zhang), Springer, Berlin, **2014**.
- [7] X. Moya, S. Kar-Narayan, N. D. Mathur, *Nat. Mater.* **2014**, *13*, 439.
- [8] Y. Liu, J. F. Scott, B. Dkhil, *Appl. Phys. Rev.* **2016**, *3*, 031102.
- [9] Z. Kutnjak, B. Rožič, R. Pirc, “Electrocaloric Effect: Theory, Measurements, and Applications” in *Wiley Encyclopedia of Electrical and Electronics Engineering*, (Ed.: J. G. Webster), Wiley, Hoboken, **2015**, pp. 1–19 DOI: <https://doi.org/10.1002/047134608X.W8244>.
- [10] Y. Liu, J. F. Scott, B. Dkhil, *APL Mater.* **2016**, *4*, 064109.
- [11] Y. Bai, G.-P. Zheng, S.-Q. Shi, *Mater. Res. Bull.* **2011**, *46*, 1866.
- [12] S. Uddin, G.-P. Zheng, Y. Iqbal, R. Ubic, J. Yang, *J. Appl. Phys.* **2013**, *114*, 213519.
- [13] W. Geng, Y. Liu, X. Meng, L. Bellaiche, J. F. Scott, B. Dkhil, A. Jiang, *Adv. Mater.* **2015**, *27*, 3165–3169.
- [14] J. Peräntie, J. Hagberg, A. Uusimäki, H. Jantunen, *Phys. Rev. B* **2010**, *82*, 134119.
- [15] F. Le Goupil, A. Berenov, A.-K. Axelsson, M. Valant, N. McN. Alford, *J. Appl. Phys.* **2012**, *111*, 124109.
- [16] A. Grünebohm, T. Nishimatsu, *Phys. Rev. B* **2016**, *93*, 134101.
- [17] I. Ponomareva, S. Lisenkov, *Phys. Rev. Lett.* **2012**, *108*, 167604.
- [18] B. Li, J. B. Wang, X. L. Zhong, F. Wang, Y. K. Zeng, Y. C. Zhou, *EPL* **2013**, *102*, 47004.
- [19] M. Marathe, C. Ederer, A. Grünebohm, *Phys. Status Solidi B* **2018**, *255*, 1700308.

- [20] M. Marathe, D. Renggli, M. Sanlialp, M. O. Karabasov, V. V. Shvartsman, D. C. Lupascu, A. Grünebohm, C. Ederer, *Phys. Rev. B* **2017**, *96*, 014102.
- [21] H. H. Wu, R. E. Cohen, *J. Phys. Condens. Matter* **2017**, *29*, 485704.
- [22] H. H. Wu, R. E. Cohen, *Phys. Rev. B* **2017**, *96*, 054116.
- [23] P. D. Thacher, *J. Appl. Phys.* **1968**, *39*, 1996–2002.
- [24] J. Wang, T. Yang, K. Wei, X. Yao, *Appl. Phys. Lett.* **2013**, *102*, 152907.
- [25] Y. K. Zeng, B. Li, J. B. Wang, X. L. Zhong, W. Wang, F. Wang, Y. C. Zhou, *RSC Adv.* **2014**, *4*, 30211–30214.
- [26] V. Basso, J.-F. Gerard, S. Pruvost, *Appl. Phys. Lett.* **2014**, *105*, 052907.
- [27] Y.-B. Ma, N. Novak, J. Koruza, T. Yang, K. Albe, B.-X. Xu, *Phys. Rev. B* **2016**, *94*, 100104(R).
- [28] Y.-B. Ma, N. Novak, K. Albe, B.-X. Xu, *Appl. Phys. Lett.* **2016**, *109*, 202906.
- [29] Y.-B. Ma, B.-X. Xu, K. Albe, A. Grünebohm, Tailoring the electrocaloric effect by internal bias fields and the field protocol, **2018**, <https://arxiv.org/pdf/1805.04380>, accessed 08 July 2018.
- [30] R. Pirc, B. Rožič, J. Koruza, B. Malič, Z. Kutnjak, *EPL* **2014**, *107*, 17002.
- [31] E. Birks, M. Dunce, J. Peräntie, J. Hagberg, A. Sternberg, *J. Appl. Phys.* **2017**, *121*, 224102.
- [32] M. E. Lines, A. M. Glass, *Principles and Applications of Ferroelectrics and Related Materials*, OUP, Oxford, **1977**.
- [33] D. C. Lupascu, I. Anusca, M. Etier, Y. Gao, G. Lackner, A. Nazrabi, M. Sanlialp, H. Trivedi, N. Ul-Haq, J. Schröder in *Ferroc Functional Material, CISM International Centre for Mechanical Sciences, Vol. 581* (Eds.: J. Schröder, D. C. Lupascu), Chap. Semiconductor Effects in Ferroelectrics, pp. 97–178, Springer, Cham, **2018**.
- [34] A. Planes, L. Mañosa, M. Acet, *J. Phys. Condens. Matter* **2009**, *21*, 233201.
- [35] A. Planes, T. Castán, A. Saxena, *Phil. Mag.* **2014**, *94*, 1893.
- [36] D. Bolten, U. Böttger, T. Schneller, M. Grossmann, O. Lohse, R. Waser, *Appl. Phys. Lett.* **2000**, *77*, 3830–3832.
- [37] M. Marathe, A. Grünebohm, T. Nishimatsu, P. Entel, C. Ederer, *Phys. Rev. B* **2016**, *93*, 054110.
- [38] M. Rose, R. E. Cohen, *Phys. Rev. Lett.* **2012**, *109*, 187604.
- [39] A.-K. Axelsson, F. L. Goupil, L. J. Dunne, G. Manos, M. Valant, N. M. Alford, *Appl. Phys. Lett.* **2013**, *102*, 102902.
- [40] Y.-B. Ma, A. Grünebohm, K.-C. Meyer, K. Albe, B.-X. Xu, *Phys. Rev. B* **2016**, *94*, 094113.
- [41] T. Limboeck, E. Soergel, *Appl. Phys. Lett.* **2014**, *105*, 152901.
- [42] B. Jaffe, W. R. Cook, H. Jaffe, *Piezoelectric Ceramics*, Academic, London, **1971**.
- [43] W. A. Schulze, K. Ogino, *Ferroelectrics* **1988**, *87*, 361–377.
- [44] D. M. Smyth, *Curr. Opin. Solid State Mater. Sci.* **1996**, *1*, 692–697.
- [45] C. Elissalde, J. Ravez, *J. Mater. Chem.* **2001**, *11*, 1957–1967.
- [46] V. Gopalan, V. Dierolf, D. A. Scrymgeour, *Annu. Rev. Mater. Res.* **2007**, *37*, 449–489.
- [47] Y. A. Genenko, J. Glaum, M. J. Hoffmann, K. Albe, *Mater. Sci. Eng. B* **2015**, *192*, 52–82.
- [48] G. Arlt, H. Neumann, *Ferroelectrics* **1988**, *87*, 109–120.
- [49] W. L. Warren, K. Vanheusden, D. Dimos, G. E. Pike, B. A. Tuttle, *J. Am. Ceram. Soc.* **1996**, *79*, 536–538.
- [50] X. Ren, *Nat. Mater.* **2004**, *3*, 91–94.
- [51] A. Picinin, M. H. Lente, J. A. Eiras, J. P. Rino, *Phys. Rev. B* **2004**, *69*, 064117.
- [52] M. Dawber, K. M. Rabe, J. F. Scott, *Rev. Mod. Phys.* **2005**, *77*, 1083–1130.
- [53] J. V. Vehten, *Dielectric Refrigerator Using Orientable Defect Dipoles*, **1979**, US No. 4,136,525.
- [54] C. Kittel, *Phys. Rev.* **1951**, *82*, 729–732.
- [55] W. N. Lawless, *Ferroelectr. Lett. Sect.* **1993**, *15*, 27–31.
- [56] S. Lisenkov, B. K. Mani, E. Glazkova, C. W. Miller, I. Ponomareva, *Sci. Rep.* **2016**, *6*, 19590.
- [57] E. Glazkova-Swedberg, J. Cuozzo, S. Lisenkov, I. Ponomareva, *Comp. Mater. Sci.* **2017**, *129*, 44.
- [58] S. E. Reyes-Lillo, K. M. Rabe, *Phys. Rev. B* **2013**, *88*, 180102.
- [59] H.-H. Wu, J. Zhu, T.-Y. Zhang, *Phys. Chem. Chem. Phys.* **2015**, *17*, 23897–23908.
- [60] F. Zhuo, Q. Li, Q. Yan, Y. Zhang, H.-H. Wu, X. Xi, X. Chu, W. Cao, *J. Appl. Phys.* **2017**, *122*, 154101.
- [61] X.-C. Zheng, G.-P. Zheng, Z. Lin, Z.-Y. Jiang, *J. Electroceram.* **2012**, *28*, 20–26.
- [62] X. Jiang, L. Luo, B. Wang, W. Li, H. Chen, *Ceram. Int.* **2014**, *40*, 2627–2634.
- [63] A. Gupta, R. Kumar, S. Singh, *Scr. Mater.* **2018**, *143*, 5–9.
- [64] A. Peláiz-Barranco, J. Wang, T. Yang, *Ceram. Int.* **2016**, *42*, 229–233.
- [65] B. Lu, P. Li, Z. Tang, Y. Yao, X. Gao, W. Kleemann, S.-G. Lu, *Sci. Rep.* **2017**, *7*, 45335.
- [66] F. Le Goupil, J. Bennett, A.-K. Axelsson, M. Valant, A. Berenov, A. J. Bell, T. P. Comyn, N. M. Alford, *Appl. Phys. Lett.* **2015**, *107*, 172903.
- [67] W. P. Cao, W. L. Li, D. Xu, Y. F. Hou, W. Wang, W. D. Fei, *Ceram. Int.* **2014**, *40*, 9273.
- [68] “Untersuchung des elektrokalorischen Effekts in P(VDF-TrFE)/BaTiO<sub>3</sub> Kompositen”, Bachelor Thesis, University of Duisburg-Essen, **2018**.
- [69] S. Jachalke, E. Mehner, H. Stöcker, J. Hanzig, M. Sonntag, T. Weigel, T. Leisegang, D. C. Meyer, *Appl. Phys. Rev.* **2017**, *4*, 021303.
- [70] B. Hanrahan, Y. Espinal, C. Neville, R. Rudy, M. Rivas, A. Smith, M. T. Kesim, S. P. Alpay, *J. Appl. Phys.* **2018**, *123*, 124104.
- [71] C. Chen, R. Liang, Z. Liu, S. Yan, X. Nie, Z. Zhou, X. Dong, *Mater. Lett.* **2017**, *189*, 303.
- [72] Y. Zhou, Q. Lin, W. Liu, D. Wang, *RSC Adv.* **2016**, *6*, 14084.
- [73] X. Nie, S. Yan, S. Guo, F. Cao, C. Yao, C. Mao, X. Dong, G. Wang, *J. Am. Ceram. Soc.* **2017**, *100*, 5202.
- [74] M. Sanlialp, V. V. Shvartsman, M. Acosta, D. C. Lupascu, *J. Am. Ceram. Soc.* **2016**, *99*, 4022.
- [75] M. Vrabelj, H. Uršič, Z. Kutnjak, B. Rožič, S. Drnovšek, A. Benčan, V. Bobnar, L. Fulanović, B. Malič, *J. Eur. Ceram. Soc.* **2016**, *36*, 75–80.
- [76] A. Kitanovski, U. Plaznik, U. Tomc, A. Poredoš, *Int. J. Refrig.* **2015**, *57*, 288–298.
- [77] S. Crossley, N. D. Mathur, X. Moya, *AIP Adv.* **2015**, *5*, 067153.
- [78] L. Mañosa, A. Planes, M. Acet, *J. Mater. Chem. A* **2013**, *1*, 4925.
- [79] J. Liu, T. Gottschall, K. P. Skokov, J. D. Moore, O. Gutfleisch, *Nat. Mater.* **2012**, *11*, 620.
- [80] T. Krenke, E. Duman, M. Acet, E. F. Wassermann, X. Moya, L. Mañosa, A. Planes, *Nat. Mater.* **2005**, *4*, 450–454.
- [81] D. Comtesse, M. E. Gruner, M. Ogura, V. V. Sokolovskiy, V. D. Buchelnikov, A. Grünebohm, R. Arróyave, N. Singh, T. Gottschall, O. Gutfleisch, V. A. Chernenko, F. Albertini, S. Fähler, P. Entel, *Phys. Rev. B* **2014**, *89*, 184403.
- [82] V. D. Buchelnikov, V. V. Sokolovskiy, H. C. Herper, H. Ebert, M. E. Gruner, S. V. Taskaev, V. V. Khovaylo, A. Hucht, A. Dannenberg, M. Ogura, H. Akai, M. Acet, P. Entel, *Phys. Rev. B* **2010**, *81*, 094411.
- [83] V. V. Sokolovskiy, A. Grünebohm, V. D. Buchelnikov, P. Entel, *Entropy* **2014**, *16*, 4992.
- [84] Z. Xu, Z. Fan, X. Liu, X. Tan, *Appl. Phys. Lett.* **2017**, *110*, 082901.
- [85] T. Gottschall, K. P. Skokov, D. Benke, M. E. Gruner, O. Gutfleisch, *Phys. Rev. B* **2016**, *93*, 184431.
- [86] A. Aznar, P. Lloveras, M. Romanini, M. Barrio, J.-L. Tamarit, C. Cazorla, D. Errandonea, N. D. Mathur, A. Planes, X. Moya, L. Mañosa, *Nat. Commun.* **2017**, *8*, 1851.
- [87] M. Gorev, E. Bogdanov, I. N. Flerov, *Scr. Mater.* **2017**, *139*, 53.
- [88] M. Gorev, E. Bogdanov, I. N. Flerov, *J. Phys. D* **2017**, *50*, 384002.
- [89] P. Lloveras, E. Stern-Taulats, M. Barrio, J.-L. Tamarit, S. Crossley, W. Li, V. Pomjakushin, A. Planes, L. Mañosa, N. D. Mathur, X. Moya, *Nat. Commun.* **2015**, *6*, 8801.
- [90] E. Stern-Taulats, P. Lloveras, M. Barrio, E. Defay, M. Egilmez, A. Planes, J.-L. Tamarit, L. Mañosa, N. D. Mathur, X. Moya, *APL Mater.* **2016**, *4*, 091102.
- [91] L. Mañosa, D. González-Alonso, A. Planes, M. Barrio, J.-L. Tamarit, I. S. Titov, M. Acet, A. Bhattacharyya, S. Majumdar, *Nat. Commun.* **2011**, *2*, 595.
- [92] R. P. Santana, N. A. de Oliveira, P. J. von Ranke, *J. Phys. Condens. Matter* **2011**, *23*, 306003.
- [93] S. Lisenkov, I. Ponomareva, *Phys. Rev. B* **2012**, *86*, 104103.

- [94] Y. Liu, J. Wei, P.-E. Janolin, I. C. Infante, J. Kreisel, X. Lou, B. Dkhil, *Phys. Rev. B* **2014**, *90*, 104107
- [95] S. Lisenkov, B. K. Mani, J. Cuzzo, I. Ponomareva, *Phys. Rev. B* **2016**, *93*, 064108.
- [96] F. Xiao, T. Fukuda, T. Kakeshita, *Scr. Mater.* **2016**, *124*, 133.
- [97] P. Álvarez-Alonso, C. O. Aguilar-Ortiz, E. Villa, A. Nespoli, H. Florez-Zúñiga, V. A. Chernenko, *Scr. Mater.* **2017**, *128*, 36.
- [98] E. Bonnot, R. Romero, L. Mañosa, E. Vives, A. Planes, *Phys. Rev. Lett.* **2008**, *100*, 125901.
- [99] Y. Liu, I. C. Infante, X. Lou, L. Bellaiche, J. F. Scott, B. Dkhil, *Adv. Mater.* **2014**, *26*, 6132–6137.
- [100] Y. Liu, J. Wei, X. Lou, L. Bellaiche, J. F. Scott, B. Dkhil, *Appl. Phys. Lett.* **2015**, *106*, 032901.
- [101] S. Lisenkov, B. K. Mani, C. M. Chang, J. Almand, I. Ponomareva, *Phys. Rev. B* **2013**, *87*, 224101.
- [102] Y. Liu, G. Zhang, Q. Li, L. Bellaiche, J. F. Scott, B. Dkhil, Q. Wang, *Phys. Rev. B* **2016**, *94*, 214113.
- [103] M. Marathe, C. Ederer, *Appl. Phys. Lett.* **2014**, *104*, 201902.
- [104] A. Grünebohm, M. Marathe, C. Ederer, *EPL* **2016**, *115*, 47002.
- [105] G. Akcay, S. P. Alpay, G. A. Rossetti, J. F. Scott, *J. Appl. Phys.* **2008**, *103*, 024104.
- [106] H.-X. Cao, Z.-Y. Li, *J. Appl. Phys.* **2009**, *106*, 094104.
- [107] M. M. Vopson, *Solid State Commun.* **2012**, *152*, 2067–2070.
- [108] Y. Liu, L. C. Phillips, R. Mattana, M. Bibes, A. Barthélémy, B. Dkhil, *Nat. Commun.* **2016**, *7*, 11614.
- [109] X.-S. Qian, H.-J. Ye, Y.-T. Zhang, H. Gu, X. Li, C. A. Randall, Q. M. Zhang, *Adv. Funct. Mater.* **2014**, *24*, 1300–1305.
- [110] Y.-B. Ma, C. Molin, V. V. Shvartsman, S. Gebhardt, D. C. Lupascu, K. Albe, B.-X. Xu, *J. Appl. Phys.* **2017**, *121*, 024103.
- [111] T. Nishimatsu, A. Grünebohm, U. Waghmare, M. Kubo, *J. Phys. Soc. Jpn.* **2016**, *85*, 114714.
- [112] Z. Luo, S. Pojprapai, J. Glaum, M. Hoffman, *J. Am. Ceram. Soc.* **2012**, *95*, 2593–2600.
- [113] Y. Bai, X. Han, K. Ding, L.-J. Qiao, *Appl. Phys. Lett.* **2013**, *103*, 162902.
- [114] X. Zhang, J. B. Wang, B. Li, X. L. Zhong, X. J. Lou, Y. C. Zhou, *J. Appl. Phys.* **2011**, *109*, 126102.
- [115] C. Verdier, D. C. Lupascu, J. Rödel, *Appl. Phys. Lett.* **2002**, *81*, 2596–2598.
- [116] D. C. Lupascu, E. Aulbach, J. Rödel, *J. Appl. Phys.* **2003**, *93*, 5551–5556.
- [117] D. C. Lupascu, *Fatigue in Ferroelectric Ceramics and Related Issues*, Springer, Berlin, **2004**.
- [118] D. C. Lupascu, J. Rödel, *Adv. Eng. Mater.* **2005**, *7*, 882.
- [119] J. Nuffer, D. C. Lupascu, J. Rödel, *J. Eur. Ceram. Soc.* **2001**, *21*, 1421–1423.

---

Manuscript received: February 28, 2018

Revised manuscript received: April 27, 2018

Accepted manuscript online: May 14, 2018

Version of record online: August 8, 2018